Magnetogenesis from vorticity in the primordial universe

Gaurav Mukherjee

BARC-HBNI, Mumbai

EPFL Bernoulli center, Lausanne

May 2024

Outline of the talk

- Ubiquity of **rotation** and **magnetic fields** on **large and small scales**
- Unity of physics, **QCD phase diagram** and systems that traverse through it
- Quark-gluon plasma, confinement-deconfinement, hadronization in heavy-ions
- Origin of rotation and magnetic fields in ultrarelativistic **heavy-ion collisions**
- Augment the planar phase diagram, zooming in on **quark-hadron transition**
- Strategy: *Statistical Hadronization Model* aka *Hadron Resonance Gas Model*
- Rotational and magnetic field effects on thermodynamics and phase transition
- Results: **augmented QCD phase diagram** in higher dimensional phase space
- Applicability and generality: Baryo-meter, **Anemometer and Magnetometer**
- Implications for the **early universe** at the quark-hadron epoch
- Observational signatures and possible impact on **CMB** temperature anisotropy
- Outlook and research agenda: **magnetogenesis from primordial vorticity**

Magnetic fields, everywhere!

The universe seems to be immersed in magnetic fields coherent over very different distance scales and becoming more and more accessible to astronomical observation

Beyond terrestrial magnetism:
Planets, Stars, Neutron stars, Black holes
Galaxies, Galaxy clusters, Superclusters,
Filaments, Voids

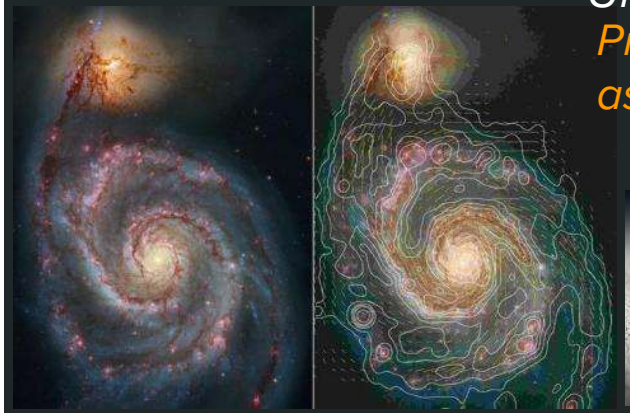

Unknown origins:
Primordial or astrophysical?
Seed field?

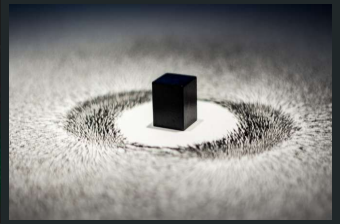

BUT WHERE DID THEY COME FROM?

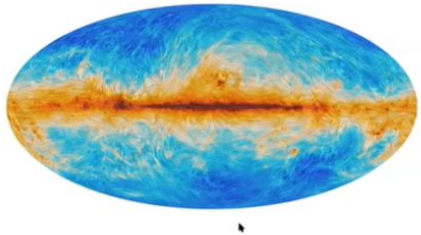

galactic B

seed field of $B \sim 10^{-20}\mathrm{G}$

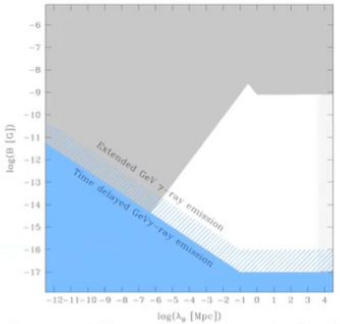

Durrer and Neronov, Astron.Astrophys.Rev. 21 (2013) 62

(hints of) extragalactic B

$10^{-15}\mathrm{G} \lesssim B \lesssim 10^{-9}\mathrm{G}$ at $\gtrsim \mathrm{Mpc}$

Large Scale Structure of the Universe: The Cosmic Web

Galaxies, Clusters, Superclusters, Filaments & Voids; Structure Formation Mechanism?

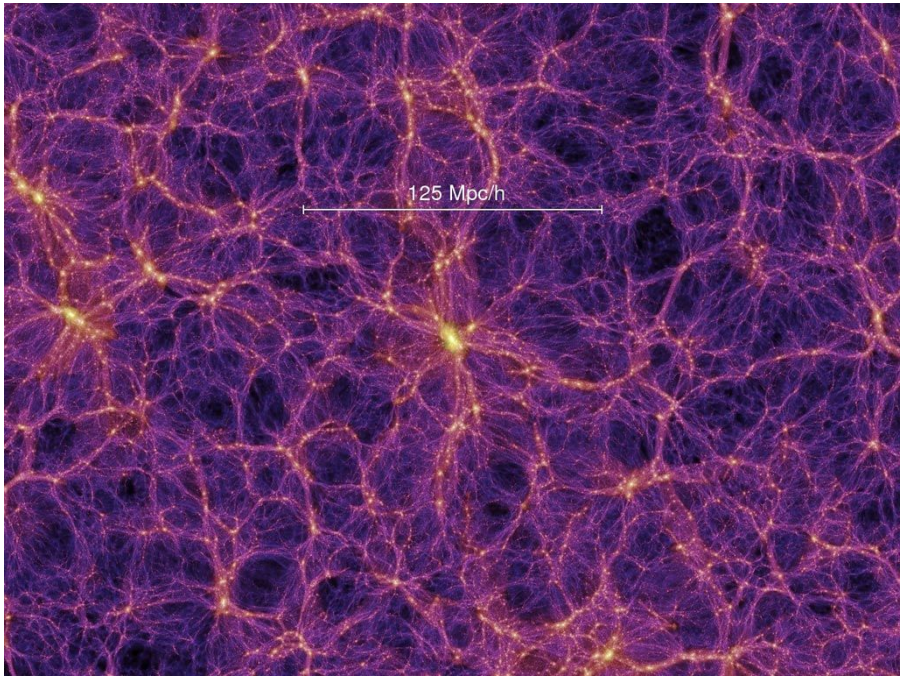

Filaments “rotating”: Angular momentum on unprecedented cosmic scales

Origin of this “spin”?

Wang et al., Nature Astro., 2021

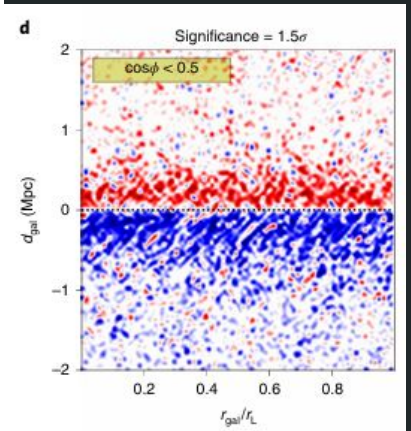

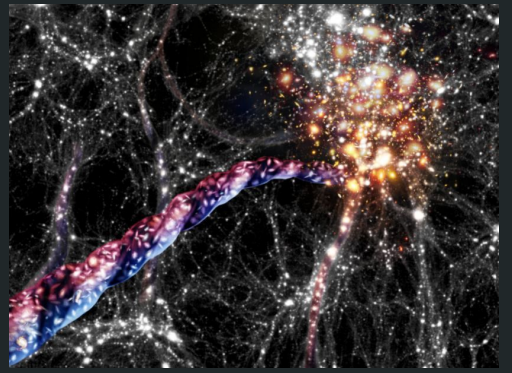

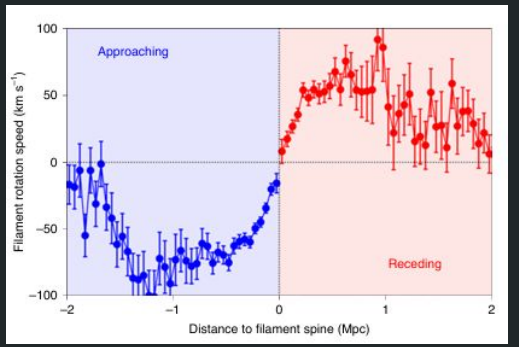

Foundations of Physics:
Quantum Field Theory & General Relativity
Standard Model of Particle Physics & Big Bang Cosmology

All fundamental interactions like the electromagnetic, strong and weak force are explained by the Standard Model and Einstein's General Theory of Relativity describes the gravitational interaction

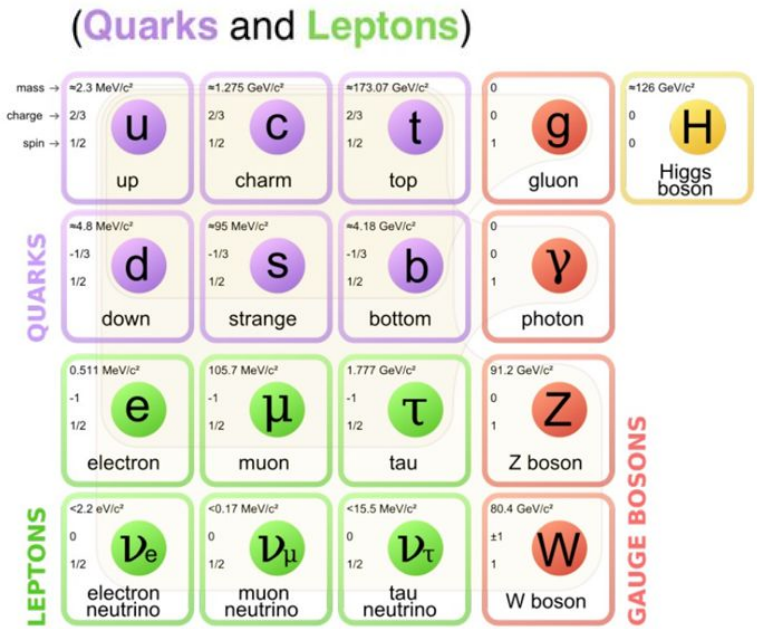

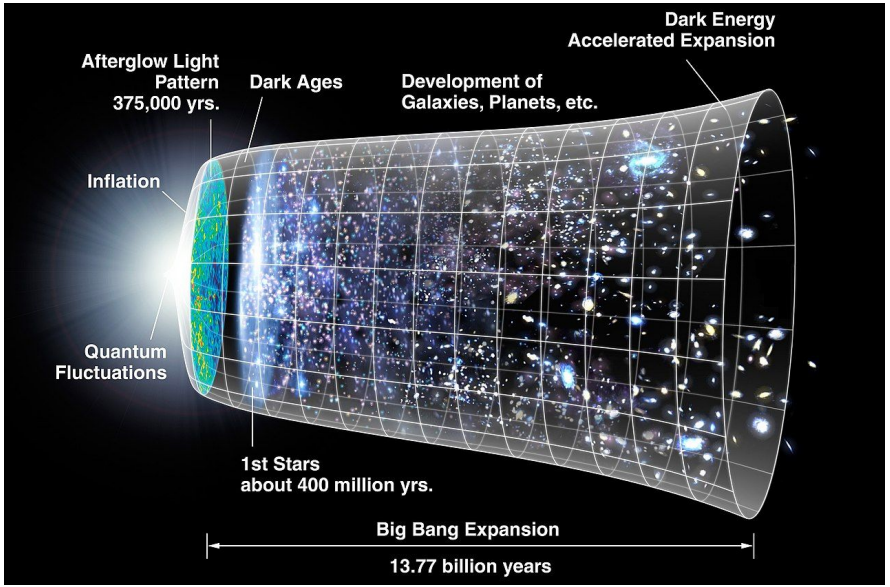

Particle accelerators to peer into the structure of matter

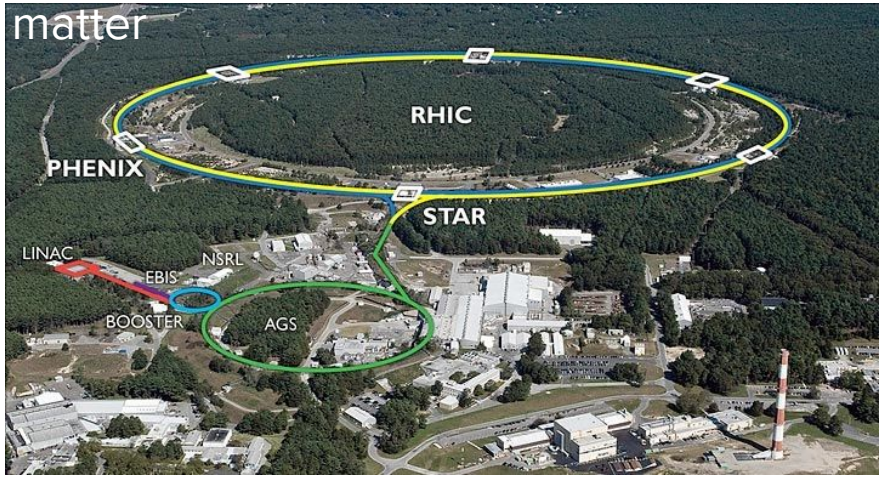

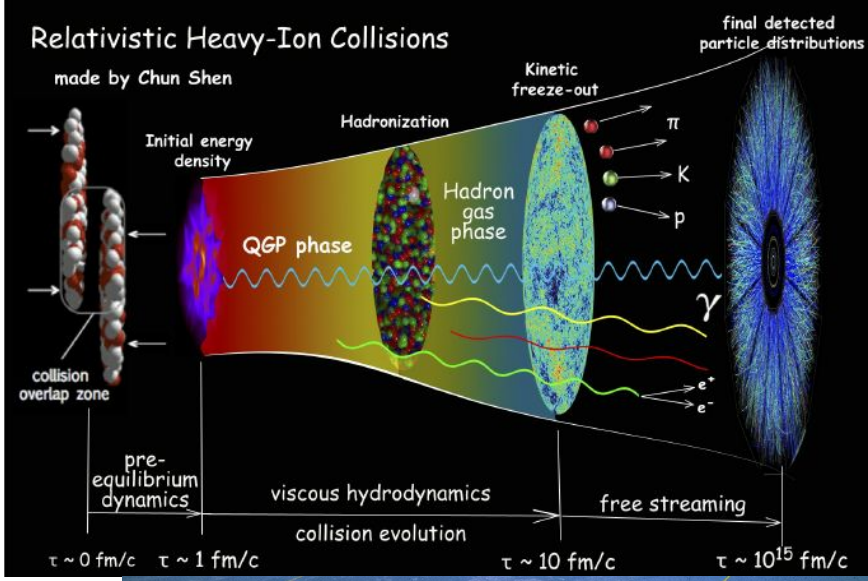

- The LHC can not only collide protons on protons, but also heavier ions.
- Approximately one month of running time is dedicated to heavy-ions each year.

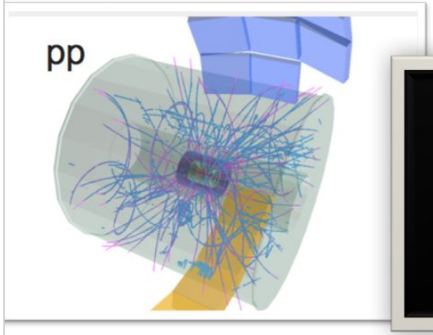

p-Pb

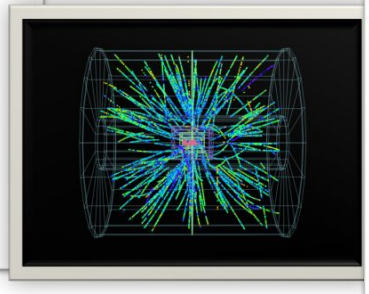

Pb-Pb

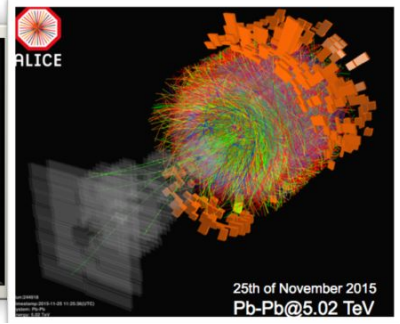

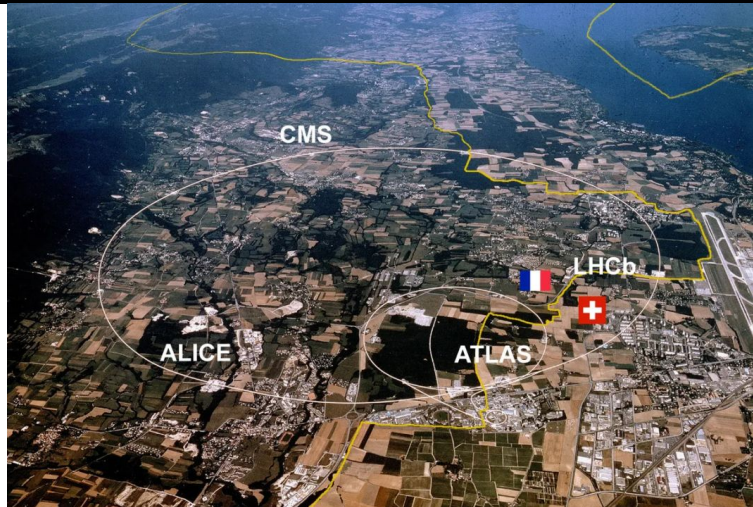

QCD, theory of the strong interaction

Quarks and gluons : fundamental constituents of QCD matter

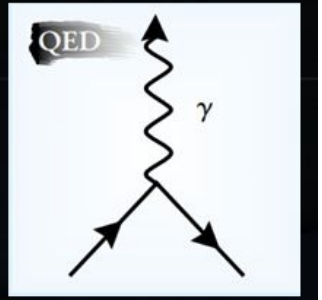

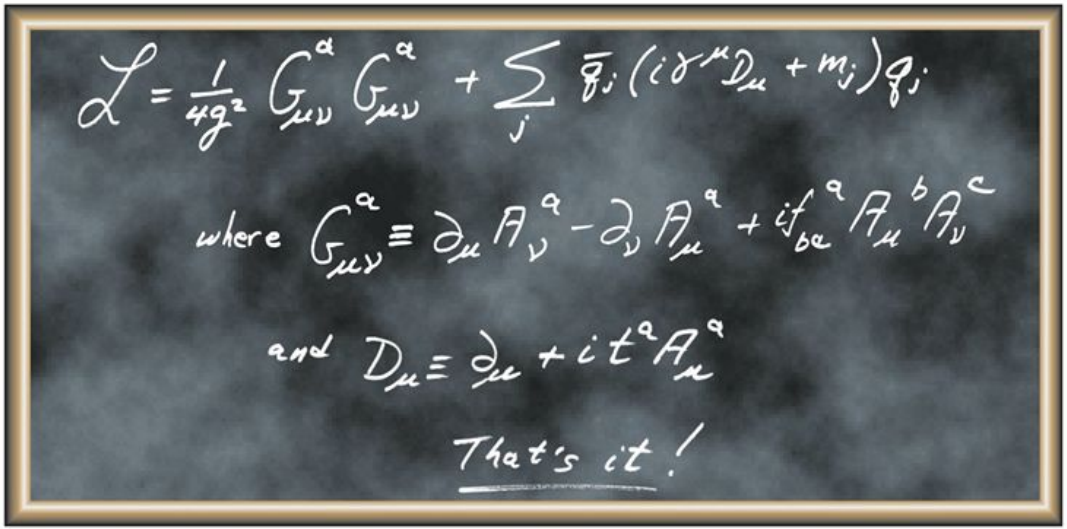

FIGURE 1. THE QCD LAGRANGIAN $\mathcal{L}$ displayed here is, in principle, a complete description of the strong interaction. But, in practice, it leads to equations that are notoriously hard to solve. Here m_j and q_j are the mass and quantum field of the quark of jth flavor, and A is the gluon field, with spacetime indices μ and ν and color indices a, b, c. The numerical coefficients f and t guarantee SU(3) color symmetry. Aside from the quark masses, the one coupling constant g is the only free parameter of the theory.

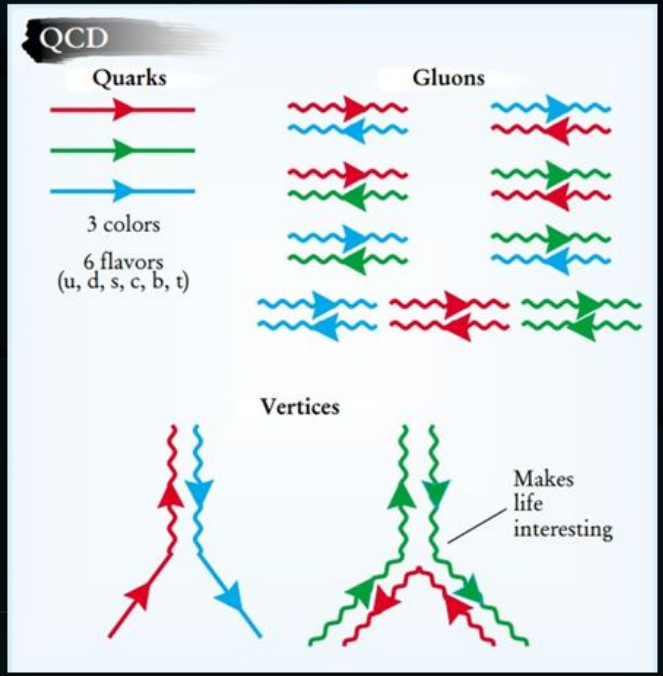

Mapping the Phases of quotidian (normal) & quantum (quark or QCD) matter

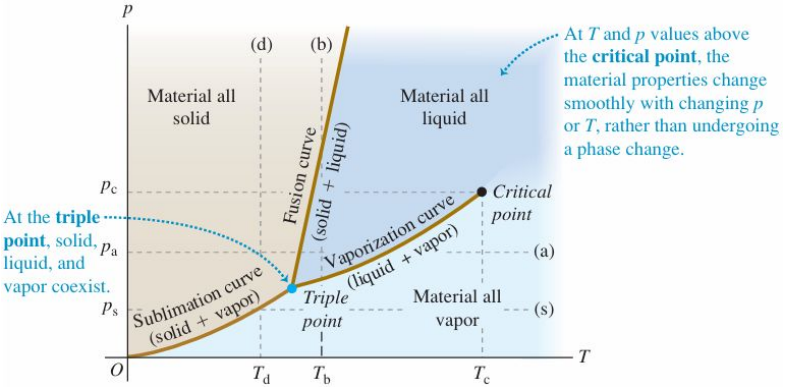

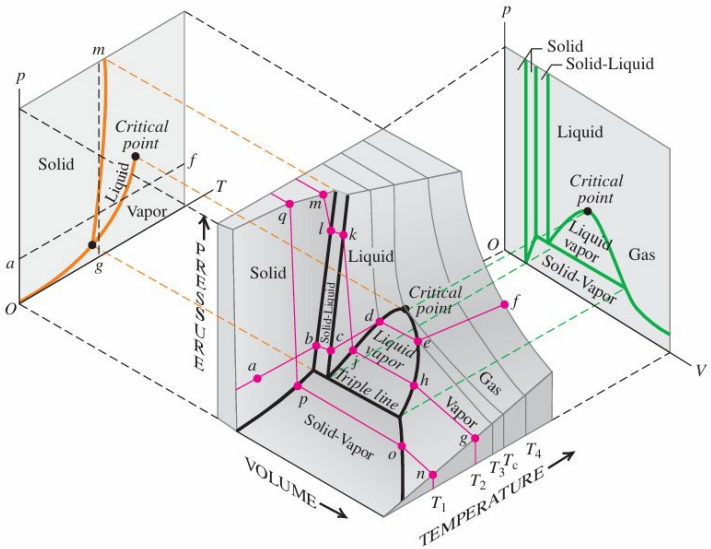

QCD phases: quark-gluon plasma (hot & dense), hadronic and nuclear matter

"Melting hadrons, boiling quarks"

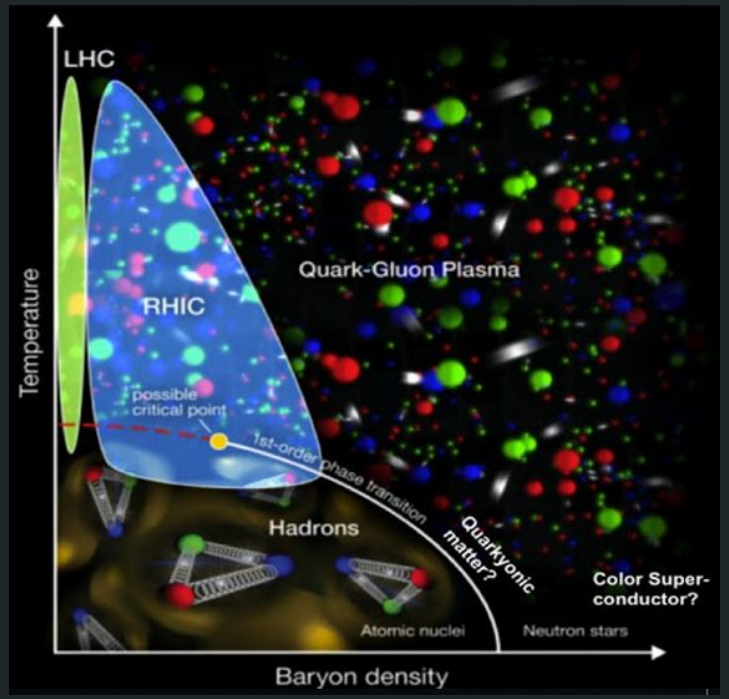

Geometry in heavy-ion collisions and the generation of vorticity & in-medium magnetic field

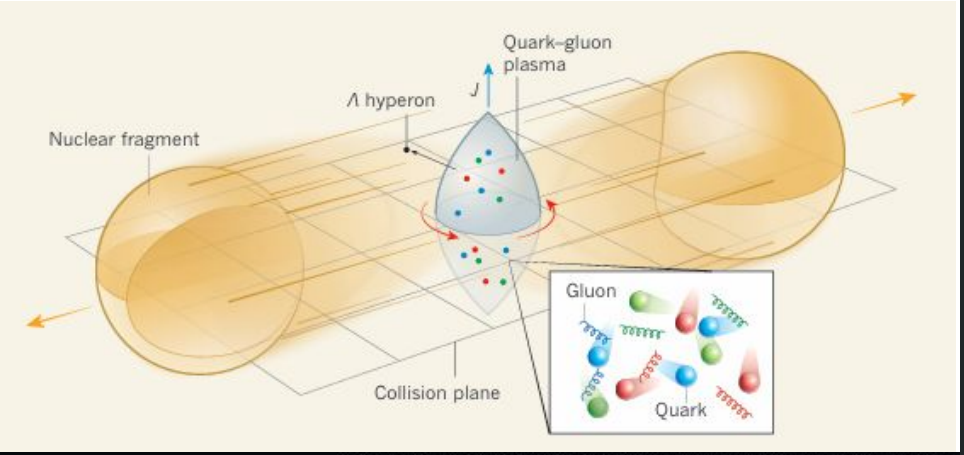

Nature Physics | VOL 15 | OCTOBER 2019 | 1040–1045

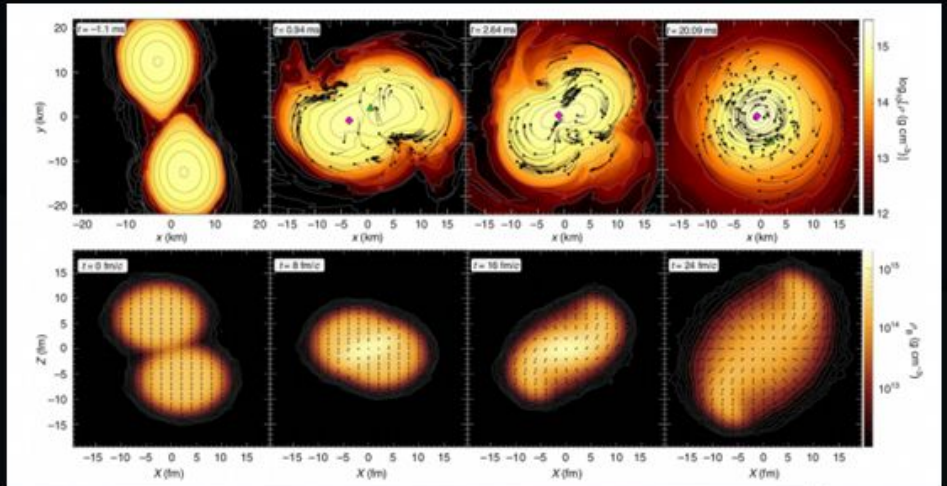

Non-central collisions: Non-zero rotation & magnetic field

Peripheral

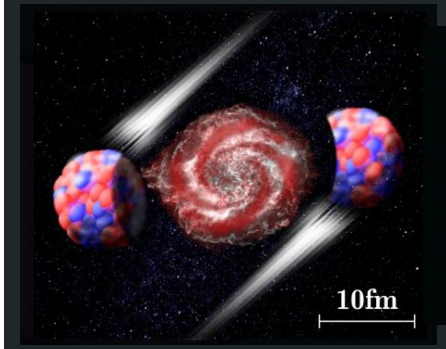

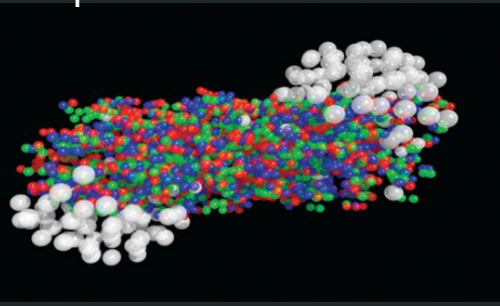

Central

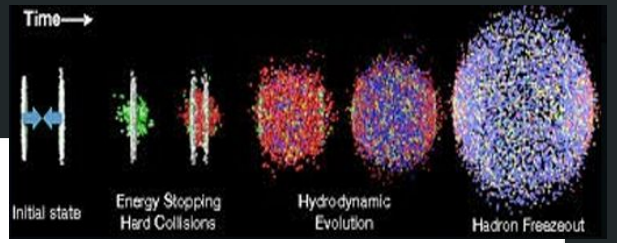

Heavy ion collision

Particle detection (t≈10^{15}fm/c)

Kinetic freeze-out (t=10fm/c)

Chemical freeze-out

Hydrodynamic evolution (t~0.5fm/c)

Pre-equilibrium

Collision (t=0fm/c)

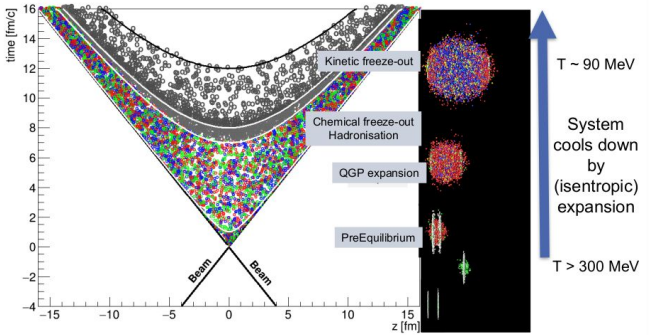

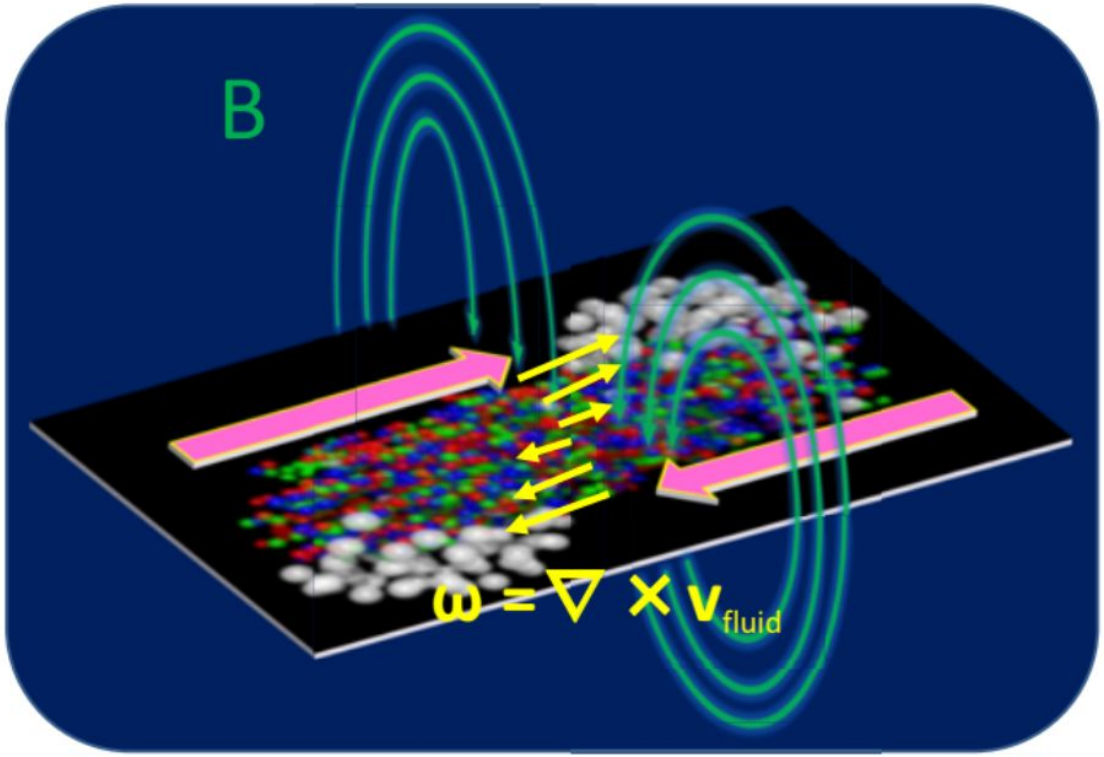

Fig. 1. Strong magnetic field and vortical field induced by the ultrarelativistic heavy-ion collisions.

*In non-central collisions, QGP droplets perform a **spinning** ballet, and have a **magnetic** personality!*

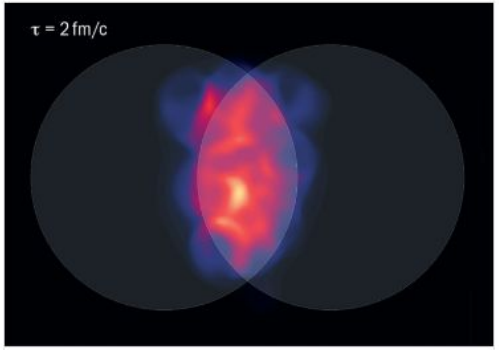

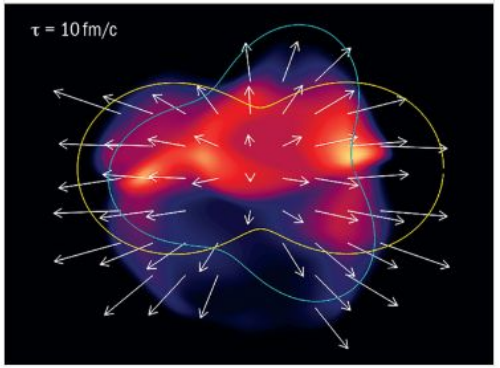

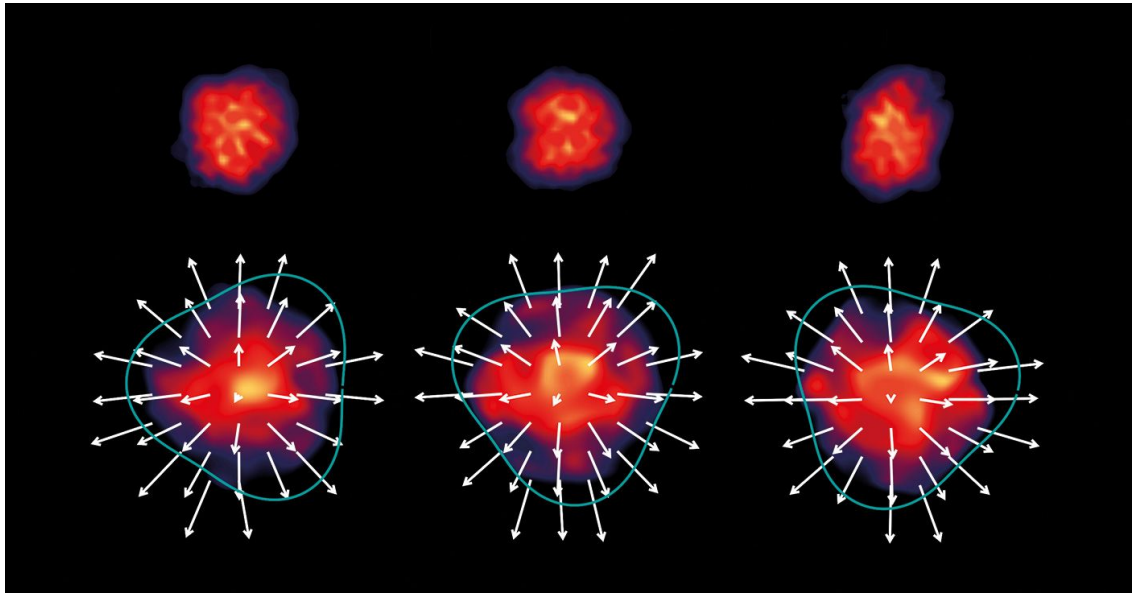

Noncentral collision An illustration of the evolving energy density of the QGP created in a noncentral collision. Pressure gradients act on the initial geometrical anisotropy to create a final velocity field (arrows), which may be decomposed into elliptic (yellow), triangular (teal) and higher order components. Hydrodynamic calculations were performed using the MUSIC software package. Credit: MUSIC arXiv:1209.6330

Transient nature of the magnetic field created by spectator nucleons

In this mechanism,

Spectator protons fly past the collision zone, creating very strong field in the overlap region where the fireball QGP droplet forms, but it is rapidly decaying

How long can the magnetic field last?

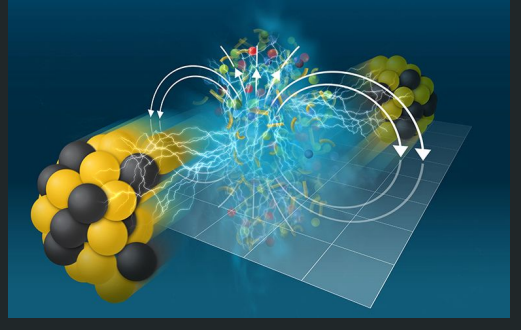

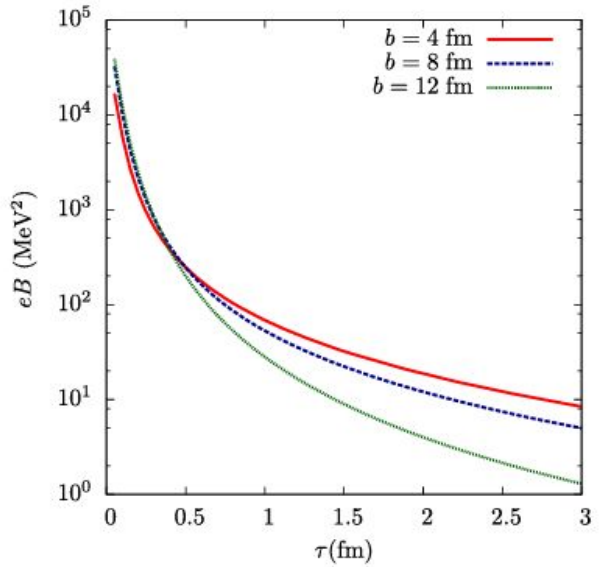

FIG. 1. Magnetic field as a function of proper time τ for three different values of the impact parameter b. From Kharzeev, McLerran, and Warringa, 2008.

Can other mechanisms extend the lifetime of the magnetic field?

Can we experimentally detect its signatures?

Yes!

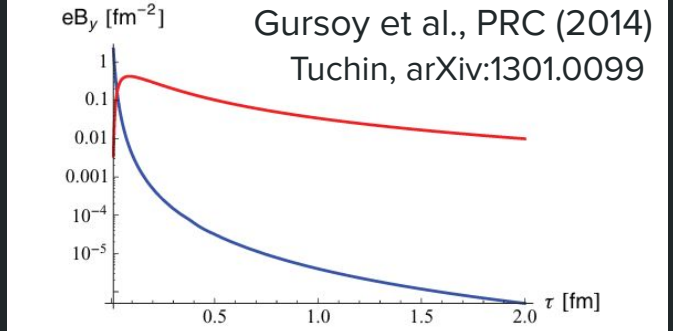

Gursoy et al., PRC (2014)
Tuchin, arXiv:1301.0099

FIG. 2. (Color online) Magnetic field B_y perpendicular to the reaction plane produced by the spectators in a heavy ion collision with impact parameter $b = 7$ fm at the LHC. The value of eB_y at the center of the collision, at $\eta = 0 = x_\perp$, is plotted as a function of τ. The blue curve shows how rapidly B_y at $\eta = 0 = x_\perp$ would decay as the spectators recede if there were no medium present, i.e., in vacuum with $\sigma = 0$. The presence of a conducting medium with $\sigma = 0.023$ fm^{-1} substantially delays the decay of B_y (red curve). At very early times before any medium has formed, when the blue curve is well above the red curve the blue curve is a better approximation.

Colossal Magnetic Field Detected in Nuclear Matter

February 23, 2024 • *Physics* 17, 31

Collisions of heavy ions briefly produced a magnetic field 10^{18} times stronger than Earth's, and it left observable effects.

Observation of the Electromagnetic Field Effect via Charge-Dependent Directed Flow in Heavy-Ion Collisions at the Relativistic Heavy Ion Collider

M. I. Abdulhamid *et al.* (STAR Collaboration)

Phys. Rev. X 14, 011028 (2024)

Published February 23, 2024

Magnetic field from Fluid Vorticity:

Charged subatomic swirl

A mechanism to generate long-lived in-medium magnetic field

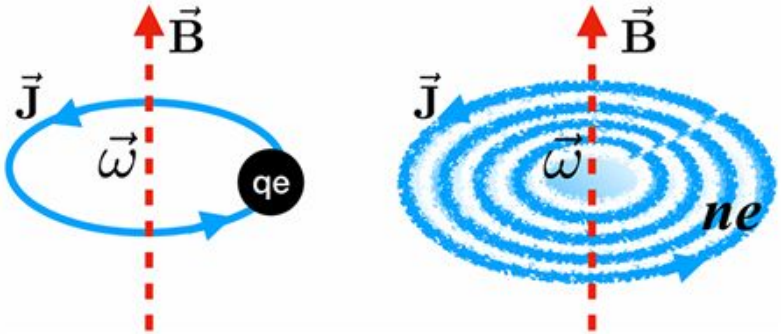

Figure 1. Illustration of the magnetic field generated by a single swirling charged particle (left) or by a swirling fluid with nonzero charge density (right).

Guo et al., 2020

Spin Hydrodynamic Generation in the charged Subatomic Swirl

- Net electric charge flows and constitutes current
- Circulating current sources magnetic field
- Angular momentum conservation
- *Persistence* of fluid vorticity, *B lifetime extended* also

$$e\overline{B} = \frac{e^2}{4\pi} n(\pi R_0^2)\,\overline{\omega} = \frac{e^2}{4\pi} n A\,\overline{\omega}$$

Augment the QCD phase diagram?

to get the full picture, where rotation parametrized by vorticity or angular velocity, and magnetic field may be non-zero simultaneously and included along with the temperature and net baryon density axes

Vorticity and magnetic field to be included

Statistical Hadronization Model aka Hadron Resonance Gas Model

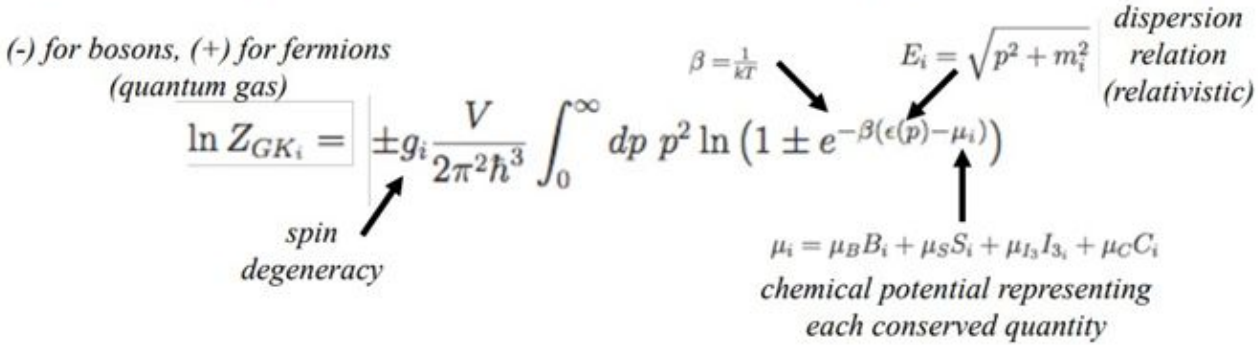

Only two free parameters are needed: (T, μ_B). Volume cancels if particle ratios n_i/n_j are calculated. If yields are fitted, it acts as the third free parameter.

Relevant interactions are mediated via resonances

Non-interacting hadron resonance gas thus serves as a good approximation for an interacting hadron gas

Thermodynamics, Deconfinement and Freeze-out

HRG model provides theoretical access to the thermodynamics, confinement-deconfinement transition and also phenomenological to heavy-ion collisions via chemical freeze-out

Once the partition function is known, we can calculate all other thermodynamic quantities:

$$n = \frac{1}{V}\frac{\partial(T\ln Z)}{\partial\mu} \quad P = \frac{\partial(T\ln Z)}{\partial V} \quad s = \frac{1}{V}\frac{\partial(T\ln Z)}{\partial T}$$

Busza et al., Annu. Rev. Nucl. Part. Sci. 2018. 68:339–76

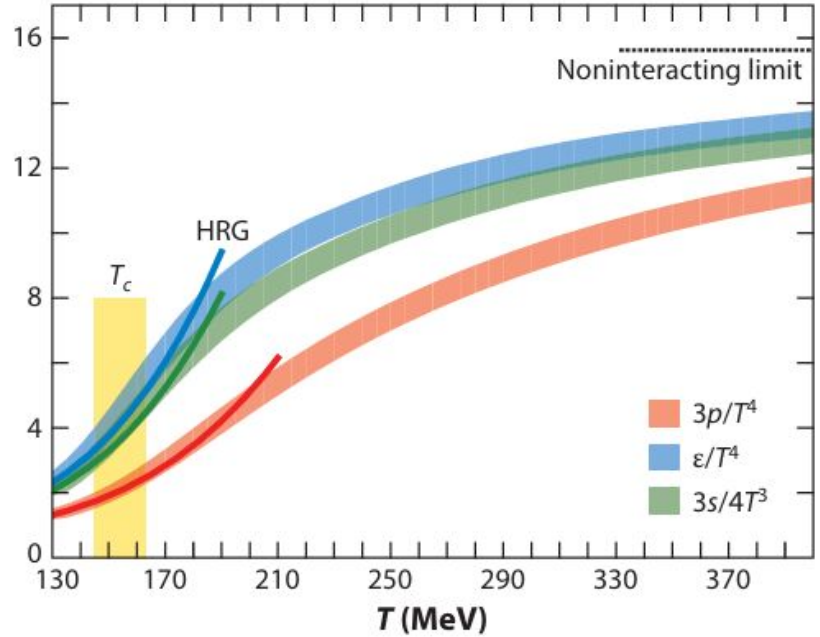

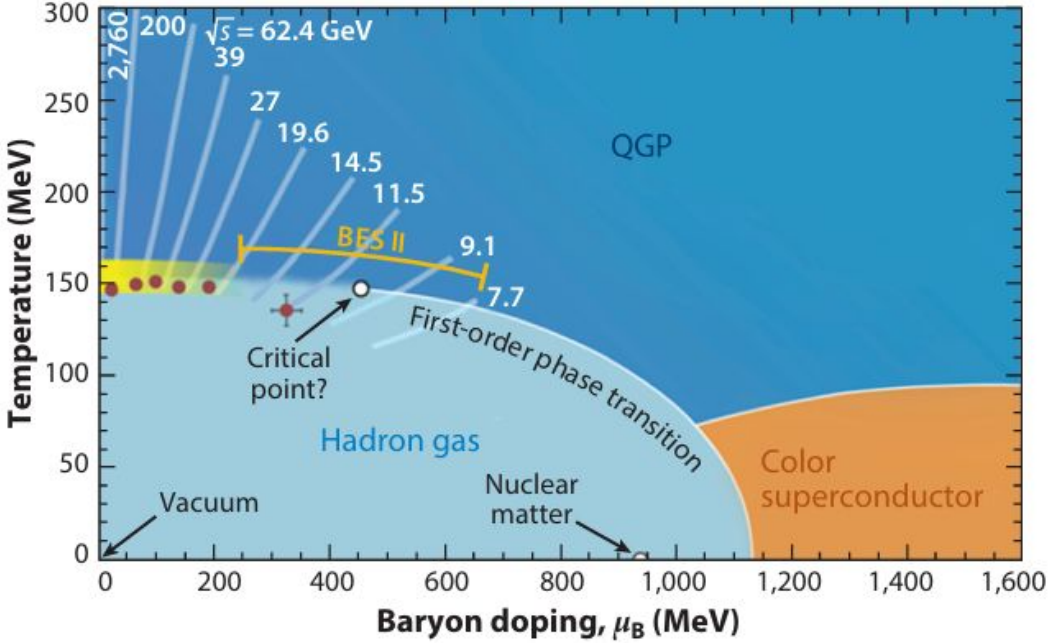

HRG model under rotation

A quantum relativistic gas of all hadrons and resonances within a cylindrical boundary obeying the causality bound (due to the speed of light constraint)

$$p_i^{\pm} = \pm \frac{T}{8\pi^2} \sum_{\ell=-\infty}^{\infty} \int dk_r^2 \int dk_z \sum_{\nu=\ell}^{\ell+2S_i} J_\nu^2(k_r r) \times \log\left\{1 \pm \exp[-(\varepsilon_{\ell,i} - \mu_i)/T]\right\}$$

$$\varepsilon_{\ell,i} = \sqrt{k_r^2 + k_z^2 + m_i^2} - (\ell + S_i)\omega$$

$$R\,\omega \leq 1$$

$$\varepsilon \geq \frac{\xi_{\ell,1}}{R} \geq \xi_{\ell,1}\,\omega$$

$$\int dk_r^2 \quad \rightarrow \quad \int_{(\Lambda_\ell^{\mathrm{IR}})^2} dk_r^2$$

$$\Lambda_\ell^{\mathrm{IR}} = \xi_{\ell,1}\omega$$

Fujimoto et al., PLB 816(2021)136184

Deconfining phase boundary under rotation

Y. Fujimoto, K. Fukushima and Y. Hidaka

Physics Letters B 816 (2021) 136184

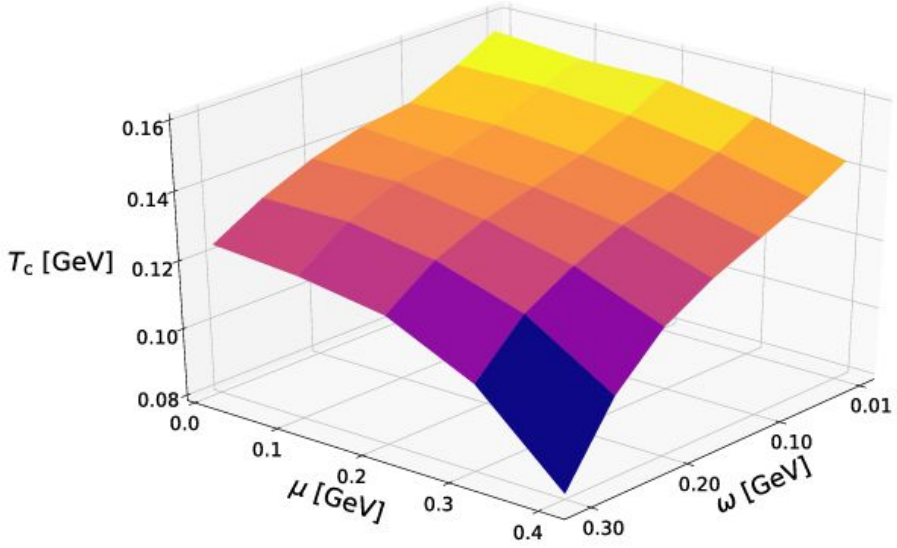

Fig. 2. Deconfinement transition surface as a function of the baryon chemical potential μ and the angular velocity ω.

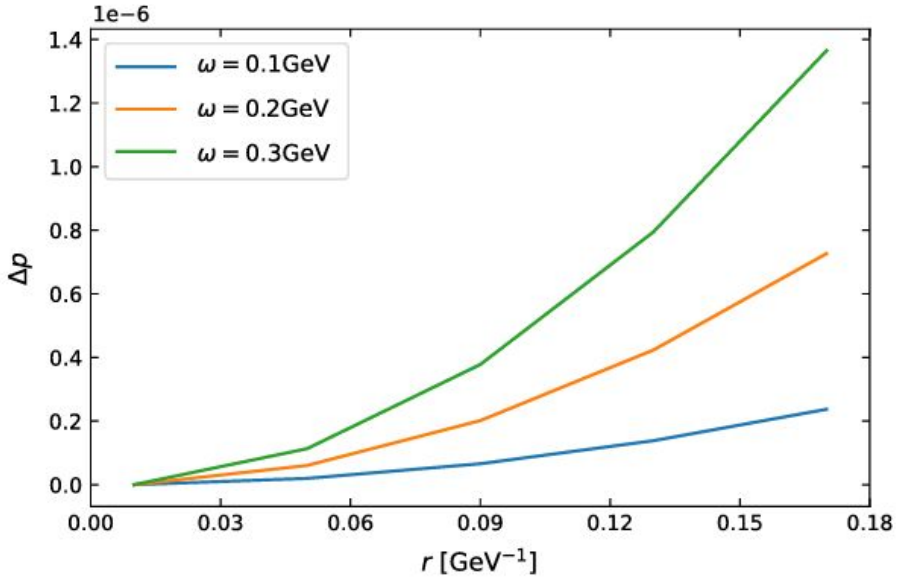

Fig. 3. Δp as a function of r for three different values of ω.

Inhomogeneity from centrifugation

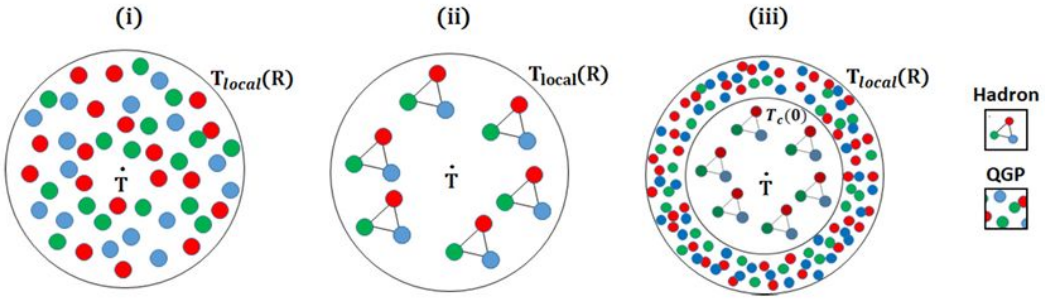

Fig. 2. Configurations of rotating QCD matter in the region $0 < \rho < R$. i) QGP without phase transition for $T > T_c(0)$. ii) Only hadronic matter for $T_c(0) > T_{local}(R)$. iii) Phase transition at ρ_c when $T_{\rm local}(\rho_c) = T_c(0)$.

Braga et al., Physics Letters B 848 (2024) 138330

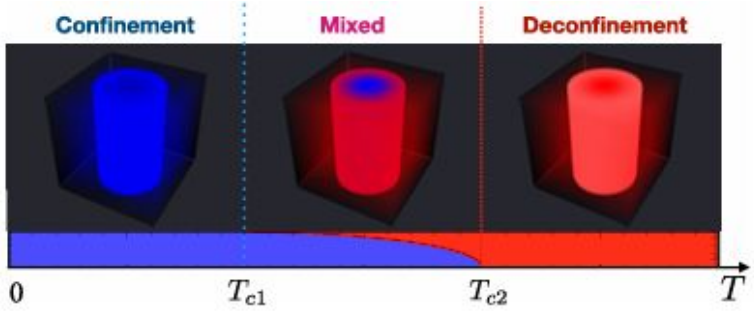

FIG. 7. Illustration of the confining, mixed, and deconfining phases of the uniformly rotating system at finite temperature.

Spatial inhomogeneity in the confined and deconfined phases from rotation even in a continuous crossover transition may manifest

Chernodub, PRD 103, 054027 (2021)

HRG model under magnetic field

A quantum relativistic gas of all hadrons and resonances embedded in a uniform magnetic field

$$f_{\rm c}(s) = \mp \sum_{s_z} \sum_{k=0}^{\infty} \frac{qB}{2\pi} \int \frac{{\rm d}p_z}{2\pi} \left(\frac{E(p_z,k,s_z)}{2} + T \log(1 \pm e^{-E(p_z,k,s_z)/T}) \right)$$

$$E(p_z,k,s_z) = \sqrt{p_z^2 + m^2 + 2qB\,(k + 1/2 - s_z)},$$

$$f_{\rm n}(s) = \mp \sum_{s_z} \int \frac{{\rm d}^3\mathbf{p}}{(2\pi)^3} \left(\frac{E_0(\mathbf{p})}{2} + T \log(1 \pm e^{-E_0(\mathbf{p})/T}) \right)$$

$$E_0(\mathbf{p}) = \sqrt{\mathbf{p}^2 + m^2}.$$

$$f^{\rm vac}(s) = f(s)|_{T=0}\,, \qquad f^{\rm therm}(s) = f(s) - f^{\rm vac}(s)$$

Endrodi, JHEP04(2013)023

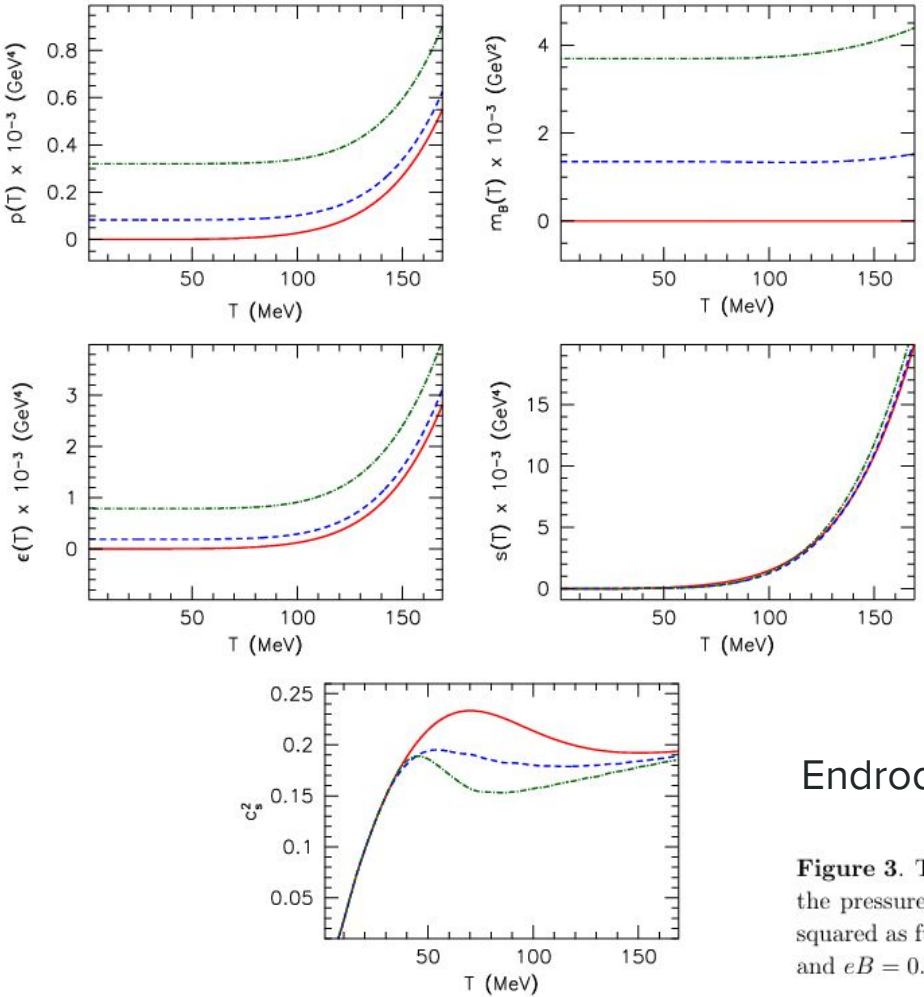

To evade divergences and renormalization calculations we can choose the entropy density and squared speed of sound to impose suitable criteria that yield the deconfinement temperature

Endrodi, JHEP04(2013)023

Figure 3. The equation of state in the HRG model. Shown are (from left to right and downwards) the pressure, the magnetization, the energy density, the entropy density and the speed of sound squared as functions of the temperature, for $eB = 0$ (solid red lines), $eB = 0.2$ GeV^2 (dashed blue) and $eB = 0.3$ GeV^2 (dot-dashed green).

HRG model under parallel rotation and magnetic field

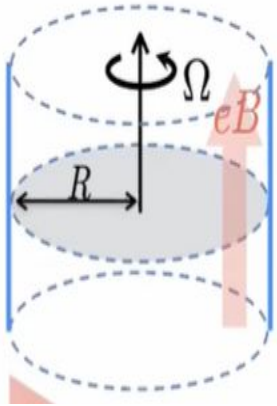

Rotation : transverse size finite

Magnetic field : Landau quantization when boundary effects can be neglected, that is, when the magnetic length is much smaller than the system size

These constraints restrict the validity of the model results to certain regimes of the various parameters.

Fortunately physical systems of interest are expected to lie in this parameter space

Strong magnetic field or weak rotation and finite size

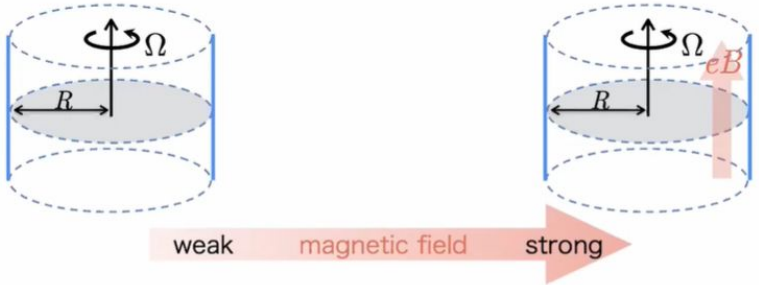

$$1/\sqrt{|Q\,B|} \ll R \lesssim 1/\omega.$$

The above inequalities may be satisfied by values relevant for a wide range of physical systems including HIC fireballs and perhaps even the early universe.

Thus this idealized model could be applicable in hitherto unexplored regimes.

Momentum Discretization

Bosons in a well

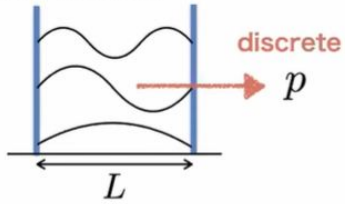

Dirichlet type

$$\sin(px)|_{x=L} = 0$$

$$\rightarrow \quad p = \frac{n\pi}{L} \geq \frac{\pi}{L}$$

IR gapped mode

Fermions in a cylinder

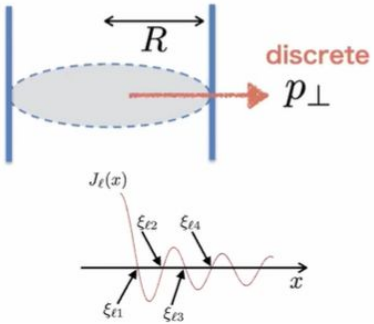

NO incoming current

$$\hat{e}_r \bar{\psi} \gamma^r \psi \Big|_{r=R} = 0$$

$$\rightarrow \quad p_\perp \mp \frac{\xi_{l,k}}{R} \geq \frac{\xi_{l,1}}{R}$$

IR gapped mode

$\xi_{l,k}$: the kth root of $J_l(x)$

Kazuya Mameda, Rotational effect versus finite-size effect
Chen et al., Phys. Rev. D 93 (10) (2016) 104052

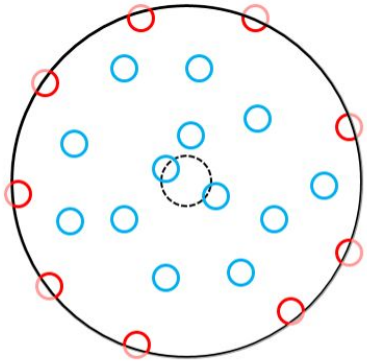

$B_1 >$

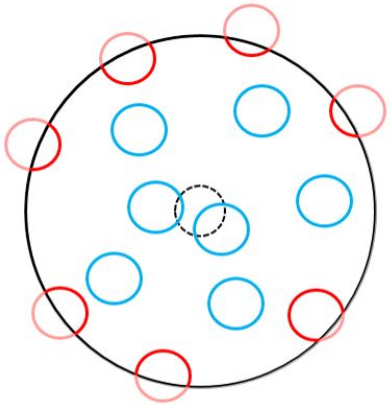

$B_2 >$

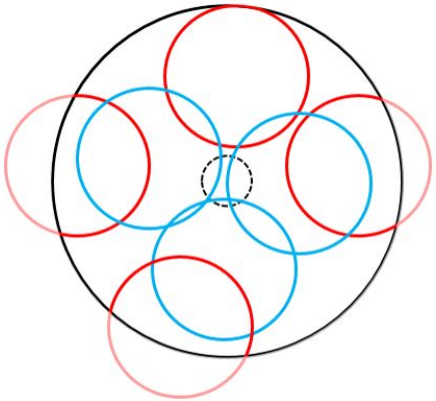

$B_3 >$

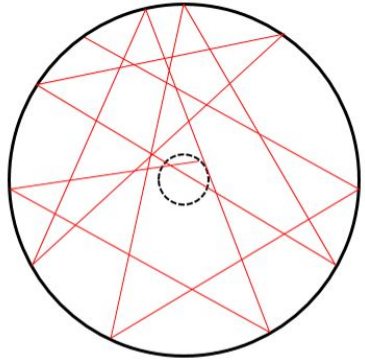

$B = 0$

$$1/\sqrt{|QB|} \ll R \leqslant 1/\omega.$$

c=1

Causality mandates boundary to maintain
Tangential velocity < Speed of light
Bulk physics unaffected by boundary for
Strong enough magnetic fields
As magnetic length, l_B << system size

Boundary conditions make finite-size effects important only when $l_{\text{system}} \lesssim l_B$ which corresponds to a very narrow sliver ($0 < eB \lesssim 0.0064$ GeV^2 for $l_B \sim l_{\text{system}} = 12.5$ GeV^{-1} or 2.5 fm) in the phase space that we will investigate. Also, these distortions occur due to the so-called edge states and become essentially irrelevant in the deep interior, i.e., $r \ll R$, of the system where only the bulk states dominate . Depicted above, schematically

Statistical Hadronization Model, aka Hadron Resonance Gas model in the presence of global vorticity & external in-medium magnetic field

$$1/\sqrt{|Q\,B|} \ll R \leqslant 1/\omega.$$

Landau quantization and Causality bound, Thermodynamic potential or free energy density

$$f_{i,c}^{b/m} = \mp \frac{T}{\pi R^2} \int \frac{dp_z}{2\pi} \sum_{n=0}^{\infty} \sum_{l=-n}^{N-n} \sum_{s_z=-s_i}^{s_i} \ln(1 \pm e^{-(\varepsilon_{i,c} - q_i\omega(l+s_z) - \mu_i)/T}), \tag{10}$$

where the dispersion relation contains the Landau levels

$$\varepsilon_{i,c} = \sqrt{p_z^2 + m_i^2 + |Q_i B|(2n - 2s_z + 1)}\ . \tag{11}$$

$$f_{i,n}^{b/m} = \mp \frac{T}{8\pi^2} \int\limits_{(\Lambda_l^{\rm IR})^2} dp_r^2 \int dp_z \sum_{l=-\infty}^{\infty} \sum_{\nu=l}^{l+2s_i} J_\nu^2(p_r r) \times \ln(1 \pm e^{-(\varepsilon_{i,n} - (l+s_i)\omega - \mu_i)/T}), \tag{12}$$

where the free part of the energy dispersion is given by

$$\varepsilon_{i,n} = \sqrt{p_r^2 + p_z^2 + m_i^2}\ . \tag{13}$$

Landau quantized spectra and the Dimensional reduction of Phase space

$$p_\perp^2 = |QB|(2n + 1 - 2s_z),\ dp_x dp_y \to 2\pi p_\perp dp_\perp = 2\pi |QB| dn$$

$$\int \frac{dp_x dp_y}{(2\pi)^2} \to \frac{|QB|}{2\pi} \sum_{n=0}^{\infty} \tag{1}$$

Landau degeneracy lifted due to Rotation

$$N = \frac{|QB|S}{2\pi},\quad S = \pi R^2$$

$$\int \frac{dp_x dp_y}{(2\pi)^2} \to \frac{1}{\pi R^2} \sum_{n=0}^{\infty} \sum_{l=-n}^{N-n} \tag{2}$$

Results: *μ, ω, eB, all finite*

Entropy density rises sharply and

Squared speed of sound dips rapidly

at deconfinement. These signal the

onset of deconfinement and can be

used as a proxy for the phase transition,

yielding the pseudo-critical or deconfinement

temperature.

GM et al., PLB846(2023)138228

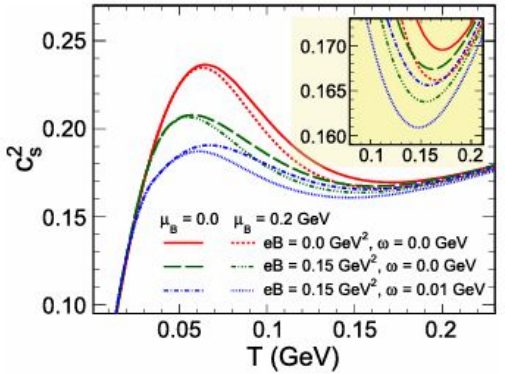

Fig. 1. The variation of the squared speed of sound as a function of temperature with a magnified view of the region where the minima occur in the inset.

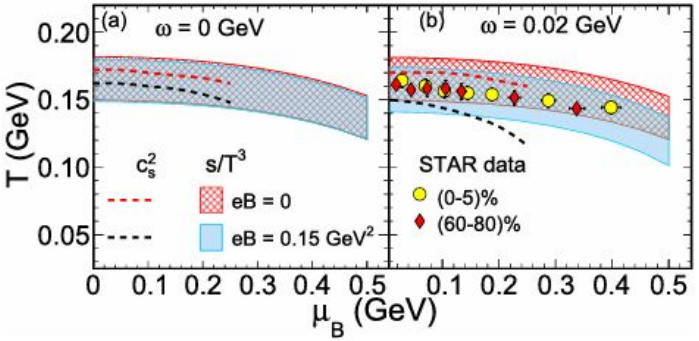

Fig. 2. QCD phase diagrams, T vs. μ_B for $eB = 0$ (red band or curve) and $eB = 0.15$ GeV^2 (blue band or curve) and (a) for $\omega = 0$ GeV and (b) for $\omega = 0.02$ GeV. The deconfinement transition zones depicted as (i) bands constrained by $s/T^3 = 4$ (lower edge) and 7 (upper edge), and (ii) curves obtained from the minima of c_s^2 vs. T as shown in Fig. 1.

Augmented QCD phase diagram

GM et al., PLB846(2023)138228

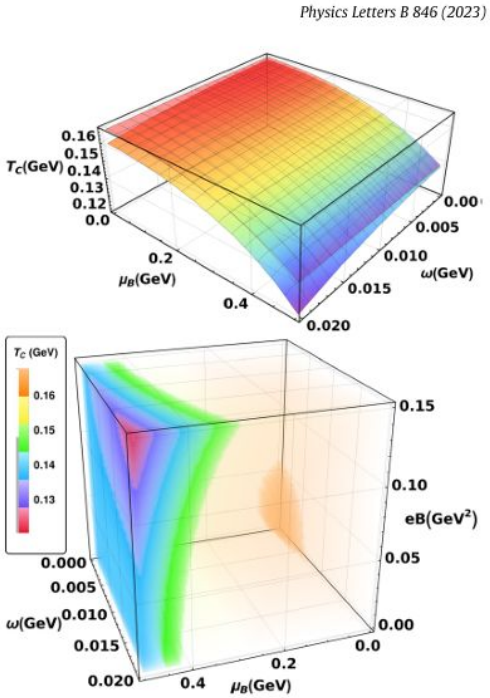

Fig. 3. (Top) Deconfinement transition surfaces showing $T_C(\mu_B,\ \omega)$ for $eB = 0$ (upper surface) and $eB = 0.15$ GeV^2 (lower surface). (Bottom) Augmented phase diagram showing $T_C(\mu_B,\ \omega,\ eB)$ as a color-coded density plot where the T_C-calibrated legend (left) provides reference for the different iso-T_C contour boundaries in the $\mu_B,\ \omega,\ eB$ space. Both plots obtained from rapid rise in entropy density at $s/T^3 = 5.5$.

Deconfinement temperature is lowered when baryon chemical potential, angular velocity and magnetic field take up finite values. These parameters seem to reinforce each other at high values where the decrease in the transition temperature is most prominent.

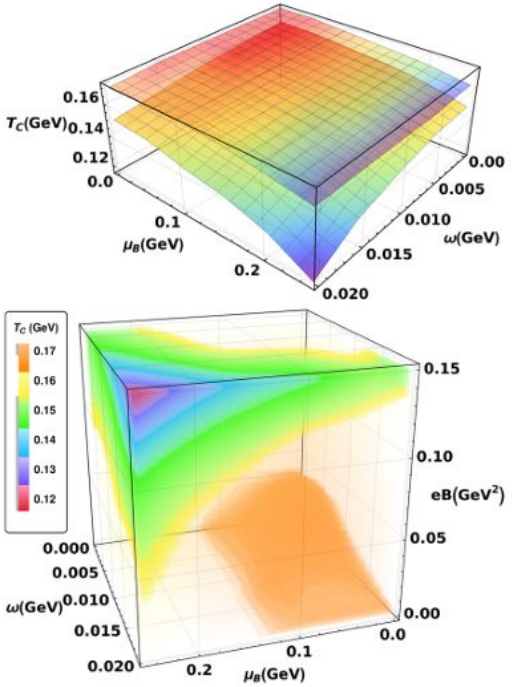

Fig. 4. (Top) Deconfinement transition surfaces showing $T_C(\mu_B,\ \omega)$ for $eB = 0$ (upper surface) and $eB = 0.15$ GeV^2 (lower surface). (Bottom) Augmented phase diagram showing $T_C(\mu_B,\ \omega,\ eB)$ as a color-coded density plot where the T_C-calibrated legend (left) provides reference for the different iso-T_C contour boundaries in the $\mu_B,\ \omega,\ eB$ space. Both obtained from the minima of the squared speed of sound.

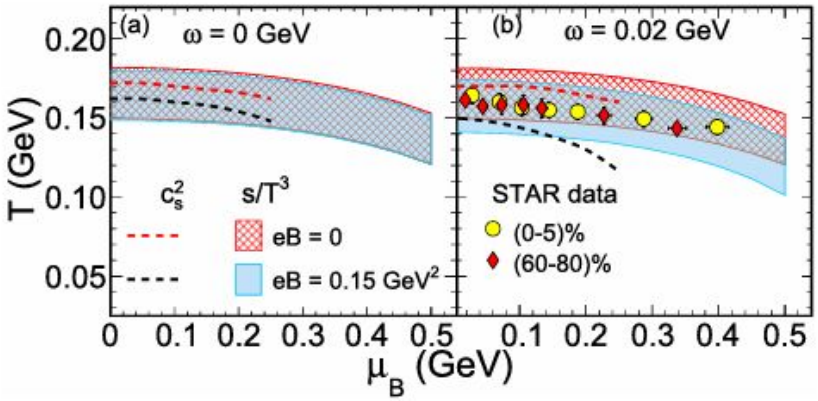

Fig. 2. QCD phase diagrams, T vs. μ_B for $eB = 0$ (red band or curve) and $eB = 0.15$ GeV^2 (blue band or curve) and (a) for $\omega = 0$ GeV and (b) for $\omega = 0.02$ GeV. The deconfinement transition zones depicted as (i) bands constrained by $s/T^3 = 4$ (lower edge) and 7 (upper edge), and (ii) curves obtained from the minima of c_s^2 vs. T as shown in Fig. 1.

In Fig. 2, we have also shown data points for chemical freezeout as extracted from experimental particle yields and ratios for two centrality classes, (0-5)% and (60-80)%. When such fitting analyses incorporate rotation and magnetic field as additional quasi-control parameters (μB , ω and eB, all dependent on collision energy and impact parameter or centrality), our phenomenological results may be better interpreted. The comparison might lead to not only T − μ freeze-out data serving as ‘thermometer’ and ‘baryometer’ but also possibly augment them with capabilities of ‘magnetometer’ and ‘anemometer’ to estimate the magnitudes of magnetic field and rotational motion prevalent in a HIC fireball. The degree of the relative influences of μ ,ω and eB might be constrained from other observable phenomena, for example measured polarization to independently constrain ω, etc.

Key findings, Conclusions

(and applications)

Simultaneous turning on of both eB and ω appears to significantly amplify the drop in T_C due to μ_B, by nearly 40 to 50 MeV

Accessing the HIC fireball properties by using this approach as a 'thermometer', 'baryometer', 'magnetometer' and 'anemometer'-like tool

The existing parameterization for chemical freeze-out data seems well-suited to be extended to include ω, eB along with T and μ_B

Implications: pronounced lowering of T_C may lead to a longer lifetime for the deconfined phase

This work may also shed some light on whether the two transition (chiral and deconfinement) temperatures stay locked in value or split as we turn on the various parameters to finite values.

HICs probe the phase space traversed by the early universe*

*along T-axis, near 0 net baryon density

The *quark-hadron transition region* that we have estimated in the phase diagram is where both

the **early universe** *passed through* and

heavy-ion collision fireball droplets *commute,* being created at particle colliders like RHIC, LHC, etc.

Could vortical fields and magnetic fields be present in the early universe too?

If yes (if they did exist in the microseconds old universe at the quark-hadron epoch), then their influence on the quark-hadron transition temperature could be important and should be taken into account

Observational constraints from the CMB may be obtained

Spatial inhomogeneity due to rotation and anisotropy from magnetic field may be important too

Evolution of the Universe: The Epochs

Modern Cosmology provides high-precision data to support this picture

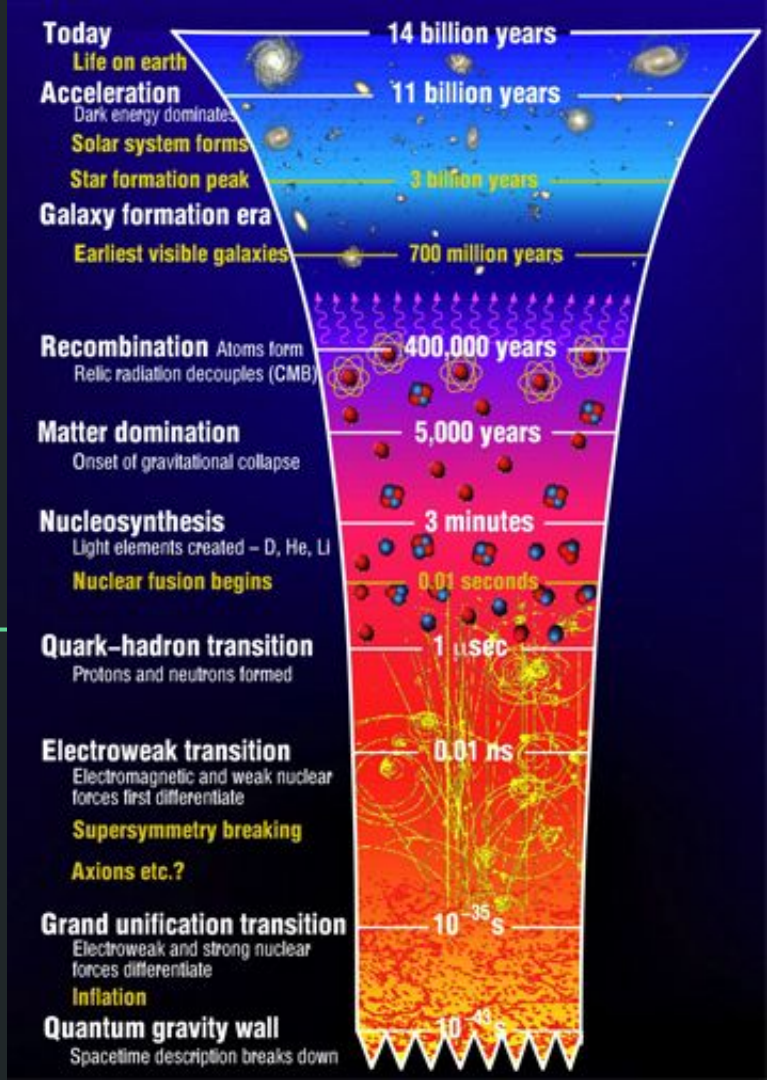

Vorticity and magnetic fields

Why can’t this be happening in the early universe?

Talks by Ruth, Tina and others explored this scenario too

1. In the quark-hadron epoch, the baryon-lepton fluid is predominantly composed of matter, not antimatter: due to prior baryogenesis
2. Baryons much heavier than leptons
3. Even quarks heavier than electrons

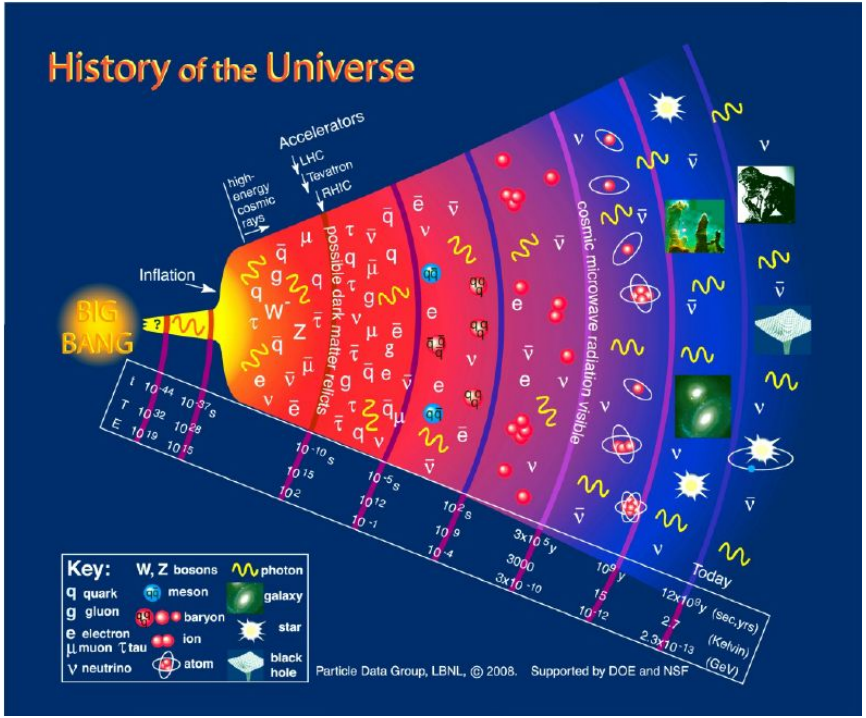

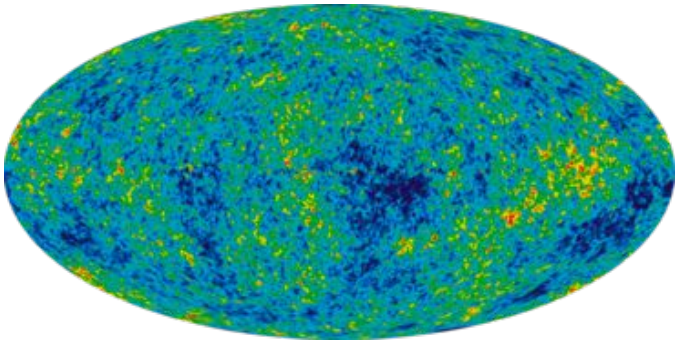

Primordial magnetogenesis:
proposed mechanism

1. Differential masses of the quarks (later baryons, mainly protons) and leptons could be responsible for a biased primordial distribution (stochastic, statistically isotropic) of local charged subatomic swirls

2. Spin hydrodynamic generation may be activated as demonstrated previously

3. Primordial magnetic fields take birth

4. The large scale magnetic fields found today may be seeded this way

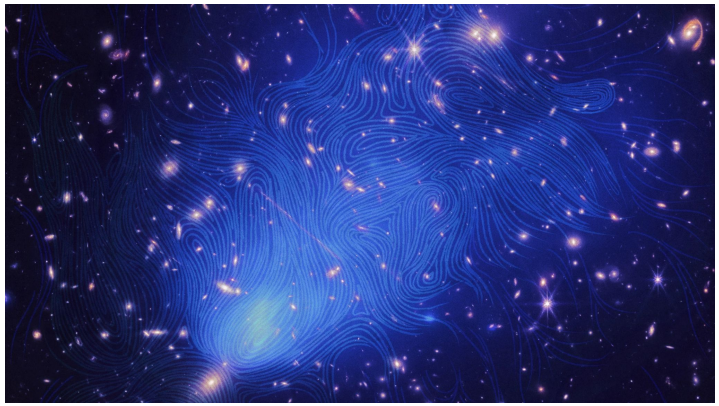

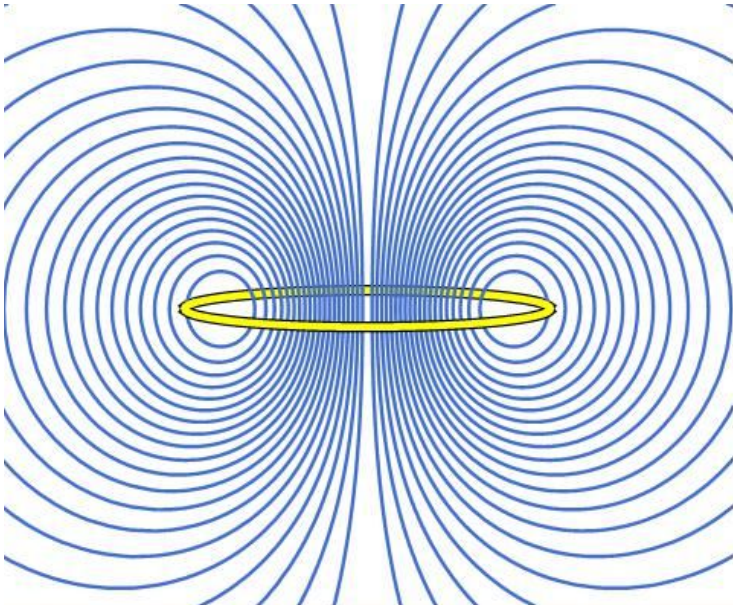

Conclusions

- We have an estimated quark-hadron deconfinement region in the QCD phase diagram that is augmented to incorporate the effects of parallel vorticity and magnetic field under ideal conditions
- This suggests in strong vortical and magnetic fields the confinement-deconfinement happens at somewhat cooler temperatures
- Heavy-ion phenomenological consequences should be important
- Experimentalists have partial control over proxies for the vorticity and magnetic field generated in HICs
- To connect with the problem of cosmological magnetogenesis and study the impact of the lowered transition temperature on the quark-hadron epoch and cosmological observables, more work is needed

Acknowledgements

D. Dutta, D. Mishra, S. Santra, R. Chaurasiya (BARC)

Jonathan, Mak, Teerthal

More to come, stay tuned!

The basic ideas appear consistent and promising

Work in progress

Expect to have complete results soon

Heavy-ion collisions to early universe (quark-hadron epoch):

Can the theoretical framework be legitimately applied throughout?
If yes, what are the parameter ranges for each case?
Where does the model break down?

1. Homogeneity and Isotropy
2. Locally violated?
3. On what scales?
4. Dynamics and evolution to present times

Thank you

Acknowledgement:

Interesting discussions with several scientists from NPD & AphD, BARC

Magnetogenesis: Alternative mechanisms

Literature contains several proposals for primordial magnetogenesis, such as

- From primordial vorticity (electron-ion plasma, not QGP; charge separation, emf, current flow, magnetic field)
- From the quark-hadron phase transition (assumed first order, which is now known not to be the case; via bubble nucleation, turbulence)
- From the electroweak phase transition
- From turbulent charge flow, Higgs field equilibration, Magnetic helicity, Electroweak baryogenesis, Inflation, Cosmic strings

Many of the above scenarios have been studied in the literature

References

https://atlas.cern/Discover/Physics

https://www.youtube.com/watch?v=m21016M8BgU&t=675s

https://cerncourier.com/a/going-with-the-flow/

https://phys.org/news/2011-05-cosmic-magnetic-fields.html

https://www.caltech.edu/about/news/caltech-astronomers-unveil-distant-protogalaxy-connected-cosmic-web-47459

https://www.americanscientist.org/article/the-cosmic-web

https://www.ctc.cam.ac.uk/outreach/origins/big_bang_three.php

Statistical-thermal model for heavy-ion collisions

- Starting point: grand-canonical partition function for an *relativistic ideal quantum gas of hadrons* of particle type i (i = pion, proton,… → full PDG!):

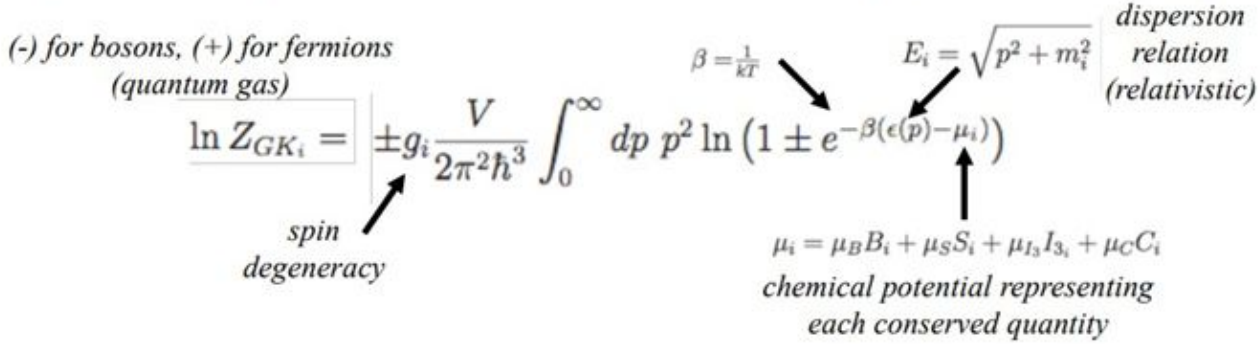

Only two free parameters are needed: **(T,μ_B)**. Volume cancels if particle ratios n_i/n_j are calculated. If yields are fitted, it acts as the third free parameter.

- Once the partition function is known, we can calculate all other thermodynamic quantities:

$$n = \frac{1}{V}\frac{\partial(T\ln Z)}{\partial\mu} \quad P = \frac{\partial(T\ln Z)}{\partial V} \quad s = \frac{1}{V}\frac{\partial(T\ln Z)}{\partial T}$$

Partition function shown here is only valid in the resonance gas limit (HRG), i.e. relevant interactions are mediated via resonances, and thus the non-interacting hadron resonance gas can be used as a good approximation for an interacting hadron gas.

Anekāntavāda, *the ultimate truth and reality is complex and has multiple aspects*

Blind men (different physics communities, like nuclear and particle physicists studying heavy-ion collisions or astrophysicists, neutron stars or cosmologists, the early universe) and an elephant (Nature with all its different aspects epitomized by the phase diagram)

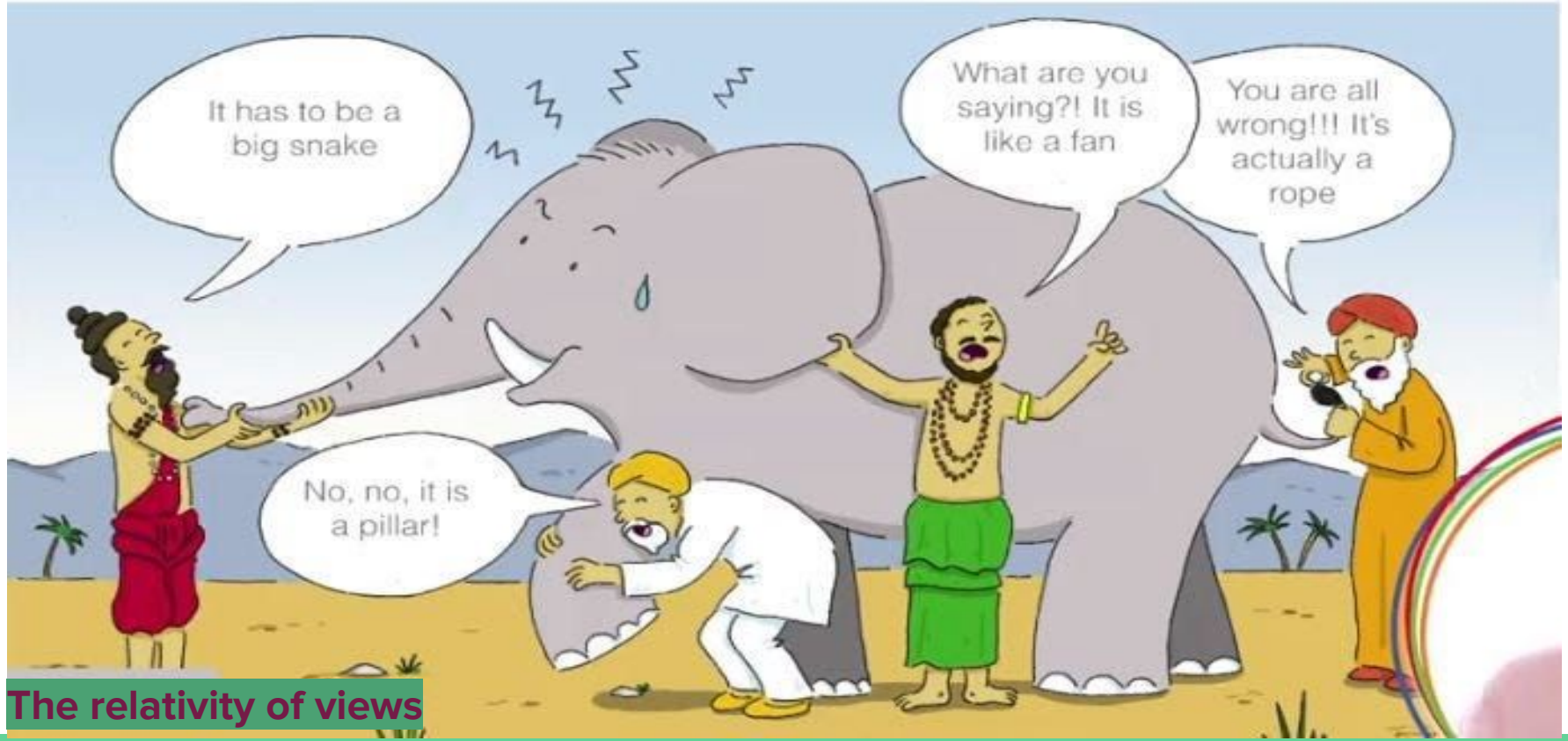

The relativity of views

What is everything made of?

Basic building blocks

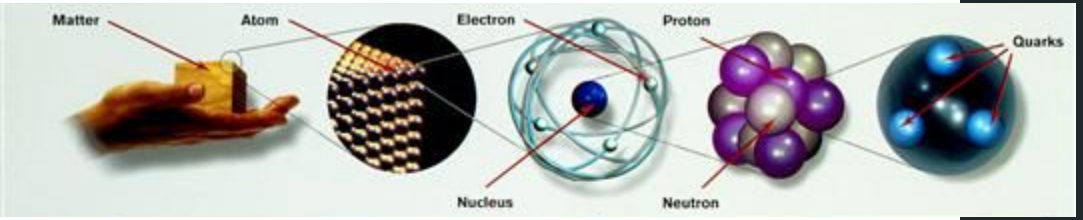

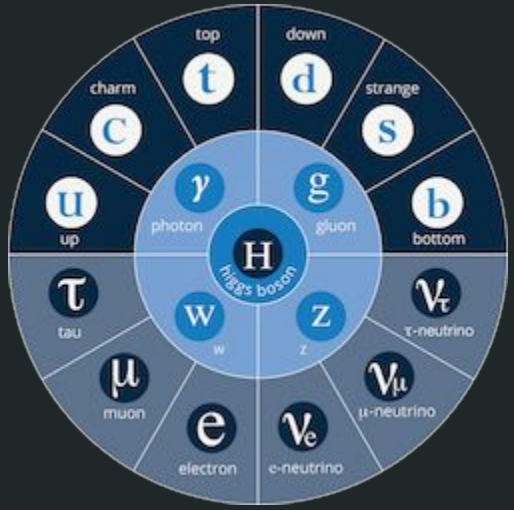

What are the contents of the universe?

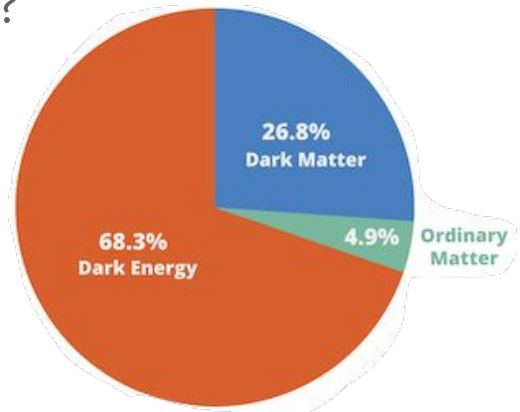

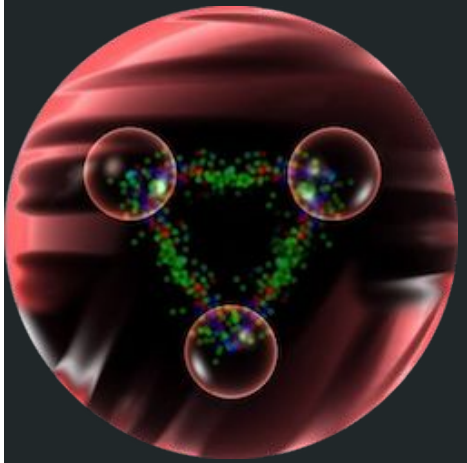

PHYS.ORG

10 hours ago

Astronomy & Space \ Astronomy

Editors' notes

A first glimpse at our galaxy's magnetic field in 3D

by Institute of Astrophysics

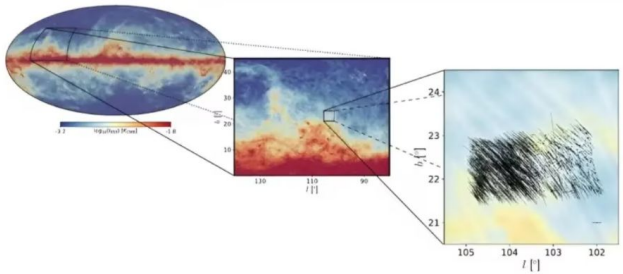

The surveyed area on the sky. Left: Full-sky map of the polarized glow emi...

Thanks to new sophisticated techniques and state-of-the-art facilities, astronomy has entered a new era in which the depth of the sky can finally be accessed. The ingredients of our cosmic home, the Milky Way galaxy—stars, gas, magnetic fields—can at long last be mapped in 3D.

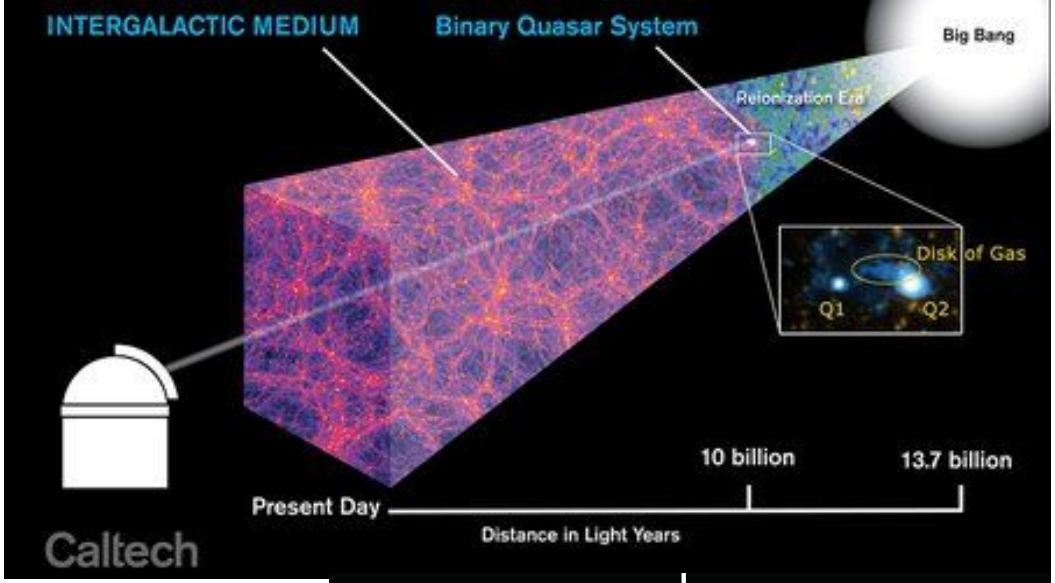

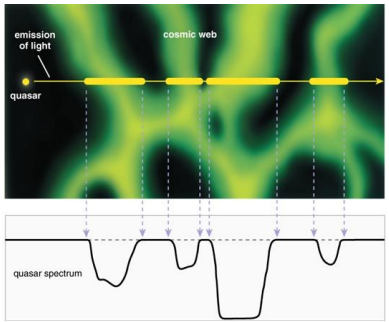

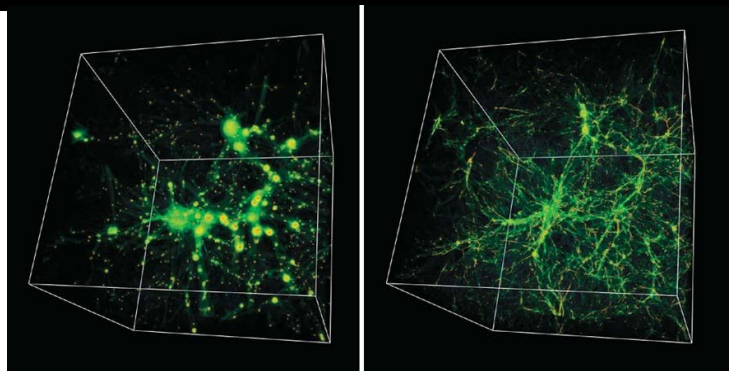

V. Pelgrims et al, The first degree-scale starlight-polarization-based tomography map of the magnetized interstellar medium, Astronomy & Astrophysics (2024). DOI: 10.1051/0004-6361/202349015

Detecting Cosmic Magnetism

Magnetic fields can't be observed directly, so researchers look for signatures of their presence. One way to do that relies on electrons traveling at near light-speed.

Synchrotron radiation

Charged particles take spiraling pathways through magnetic fields. That twisting motion generates observable radio waves.

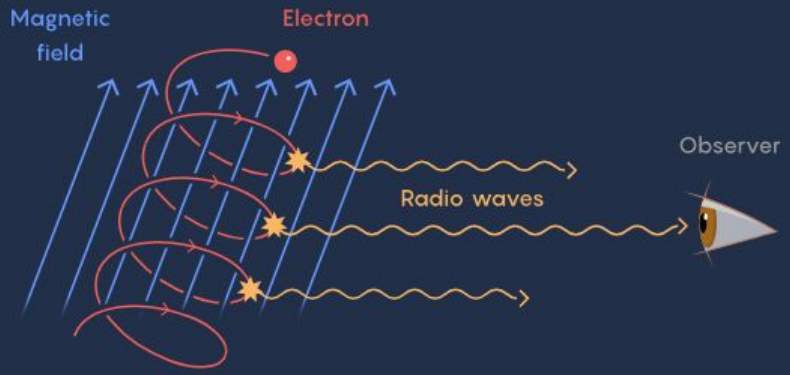

Cosmic Cartography

Scientists typically find cosmic magnetic fields by studying synchrotron radiation — radio emissions produced as a magnetic field bends the path of electrons traveling close to the speed of light. Such observations can also use the orientation of those radio emissions — their polarization — to reveal the orientation of the magnetic fields. But polarization measurements are extremely time-consuming, and work best in denser and dustier regions of a galaxy cluster.

Faraday rotation

A magnetic field rotates the polarization of light waves that pass through it.

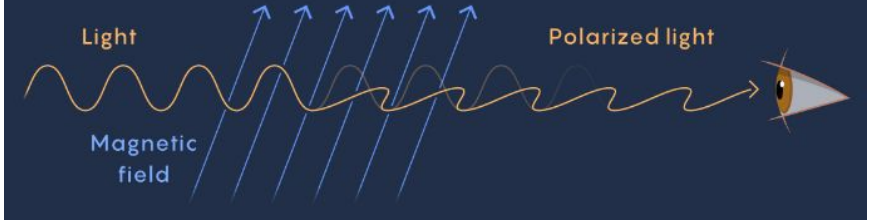

It's all relative!

A head-on collision may not be head-on in another frame.

Lorentz invariance, a spacetime symmetry under Lorentz boosts

Gauge invariance, an internal 'symmetry' responsible for electromagnetic and other Standard Model interactions

$$F_{\mu\nu} = \begin{pmatrix} 0 & B_z & -B_y & -iE_x \\ -B_z & 0 & B_x & -iE_y \\ B_y & -B_x & 0 & -iE_z \\ iE_x & iE_y & iE_z & 0 \end{pmatrix}$$

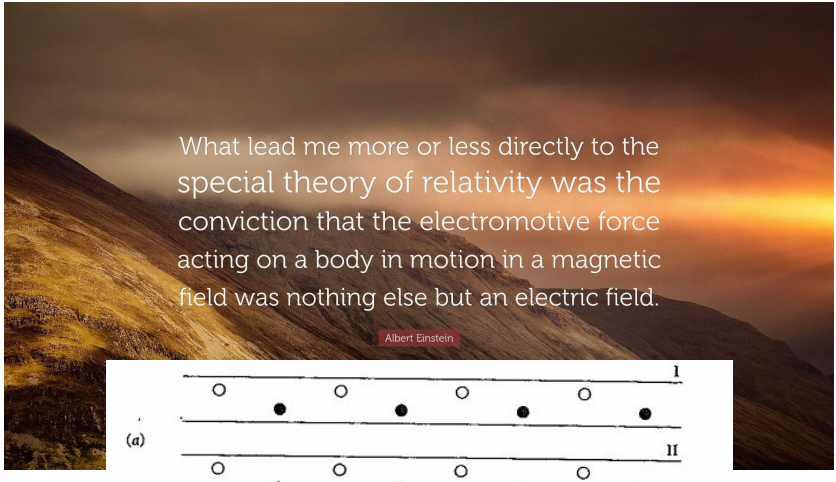

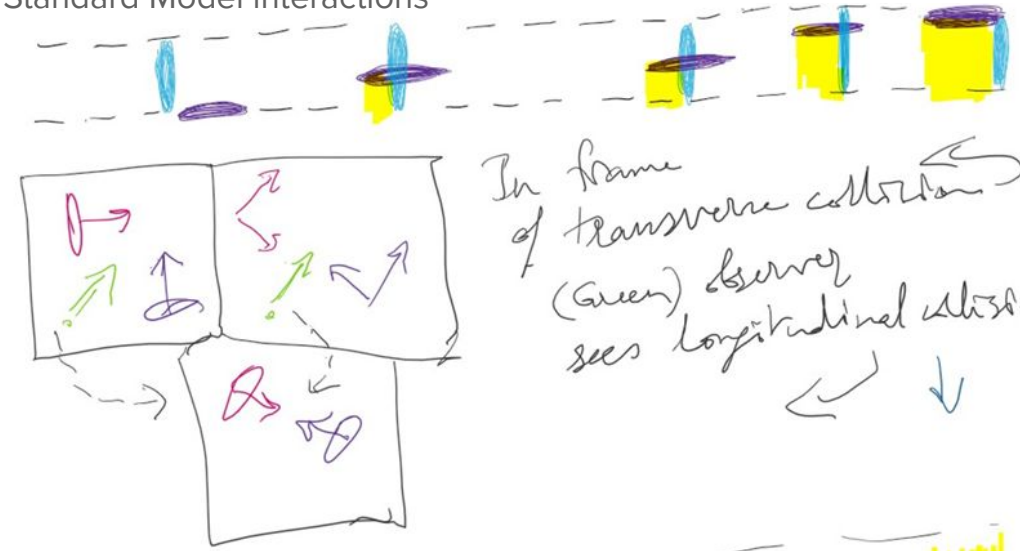

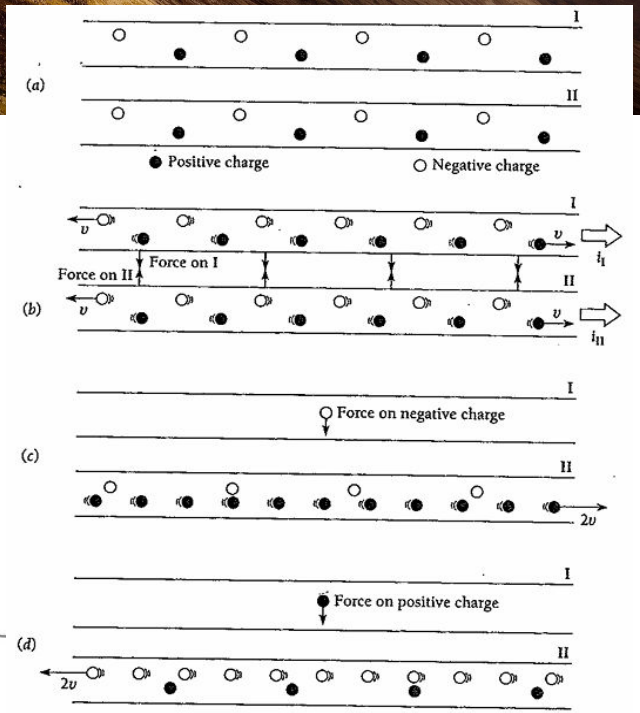

Augmented QCD Phase Portraits in 2D, 3D and 4D, from Statistical Hadronization Model

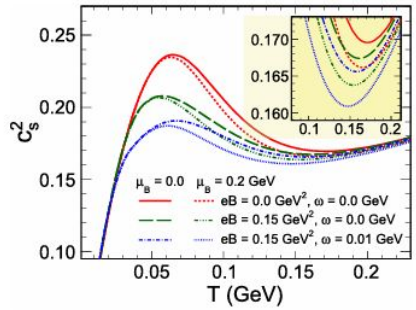

Fig. 1. The variation of the squared speed of sound as a function of temperature with a magnified view of the region where the minima occur in the inset.

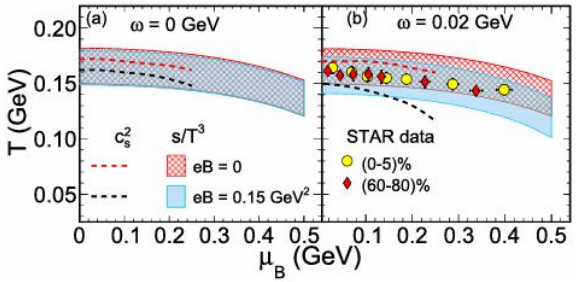

Fig. 2. QCD phase diagrams, T vs. μ_B for $eB = 0$ (red band or curve) and $eB = 0.15$ GeV^2 (blue band or curve) and (a) for $\omega = 0$ GeV and (b) for $\omega = 0.02$ GeV. The deconfinement transition zones depicted as (i) bands constrained by $s/T^3 = 4$ (lower edge) and 7 (upper edge), and (ii) curves obtained from the minima of c_s^2 vs. T as shown in Fig. 1.

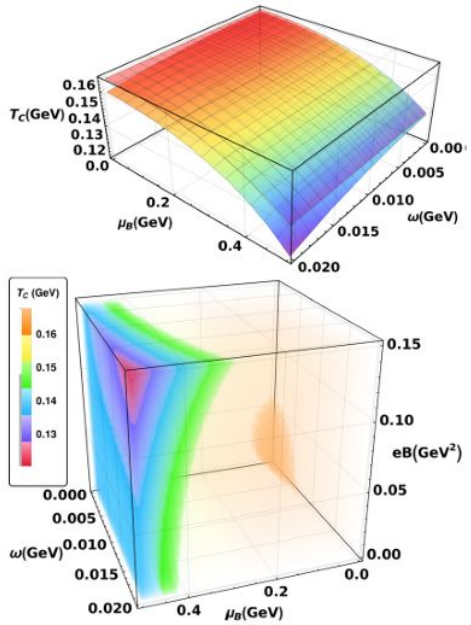

Fig. 3. (Top) Deconfinement transition surfaces showing $T_C(\mu_B,\ \omega)$ for $eB = 0$ (upper surface) and $eB = 0.15$ GeV^2 (lower surface). (Bottom) Augmented phase diagram showing $T_C(\mu_B,\ \omega,\ eB)$ as a color-coded density plot where the T_C-calibrated legend (left) provides reference for the different iso-T_C contour boundaries in the $\mu_B,\ \omega,\ eB$ space. Both plots obtained from rapid rise in entropy density at $s/T^3 = 5.5$.

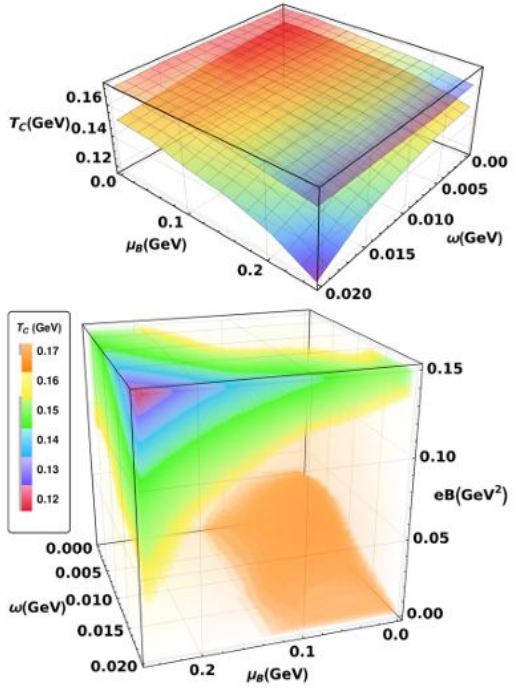

Fig. 4. (Top) Deconfinement transition surfaces showing $T_C(\mu_B,\ \omega)$ for $eB = 0$ (upper surface) and $eB = 0.15$ GeV^2 (lower surface). (Bottom) Augmented phase diagram showing $T_C(\mu_B,\ \omega,\ eB)$ as a color-coded density plot where the T_C-calibrated legend (left) provides reference for the different iso-T_C contour boundaries in the $\mu_B,\ \omega,\ eB$ space. Both obtained from the minima of the squared speed of sound.

$$\frac{\partial E_x}{\partial x} + \frac{\partial E_y}{\partial y} + \frac{\partial E_z}{\partial z} = 4\pi\rho \qquad (1)$$

$$\frac{\partial B_x}{\partial x} + \frac{\partial B_y}{\partial y} + \frac{\partial B_z}{\partial z} = 0 \qquad (2)$$

$$\left.\begin{aligned} \frac{\partial E_x}{\partial x} - \frac{\partial E_y}{\partial y} + \tfrac{1}{c}\dot{B}_z = 0 \\ \frac{\partial E_y}{\partial z} - \frac{\partial E_z}{\partial y} + \tfrac{1}{c}\dot{B}_x = 0 \\ \frac{\partial E_z}{\partial x} - \frac{\partial E_x}{\partial z} + \tfrac{1}{c}\dot{B}_y = 0 \end{aligned}\right\} \qquad (3)$$

$$\left.\begin{aligned} \frac{\partial B_x}{\partial y} - \frac{\partial B_y}{\partial x} - \tfrac{1}{c}\dot{E}_z = \tfrac{4\pi}{c} j_z \\ \frac{\partial B_y}{\partial z} - \frac{\partial B_z}{\partial y} - \tfrac{1}{c}\dot{E}_x = \tfrac{4\pi}{c} j_x \\ \frac{\partial B_z}{\partial x} - \frac{\partial B_x}{\partial z} - \tfrac{1}{c}\dot{E}_y = \tfrac{4\pi}{c} j_y \end{aligned}\right\} \qquad (4)$$

Original form

$$\nabla \cdot \mathbf{E} = 4\pi\rho \qquad (1)$$

$$\nabla \cdot \mathbf{B} = 0 \qquad (2)$$

$$\nabla \times \mathbf{E} + \tfrac{1}{c}\dot{\mathbf{B}} = 0 \qquad (3)$$

$$\nabla \times \mathbf{B} - \tfrac{1}{c}\dot{\mathbf{E}} = \tfrac{4\pi}{c}\mathbf{j} \qquad (4)$$

Simplified using rotational symmetry

$$\partial_\nu F^{\mu\nu} = \tfrac{4\pi}{c} j^\mu \qquad (1 \text{ and } 4)$$

$$\varepsilon^{\mu\nu\kappa\lambda}\,\partial_\nu F_{\kappa\lambda} = 0 \qquad (2 \text{ and } 3)$$

Further simplified using the symmetry of special relativity

QGP *toh* QGP *hota hai!**

*conditions apply

Our estimate of the *quark-hadron transition region* in the hot and zero-to-small net baryon density region of the phase diagram is where both

the **early universe** passed through(!) and

heavy-ion collision fireball droplets commute

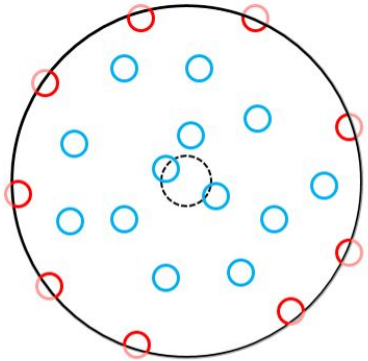

$B_1 >$

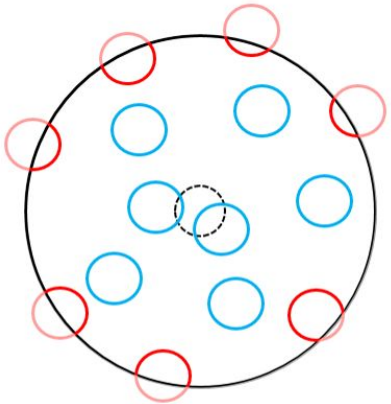

$B_2 >$

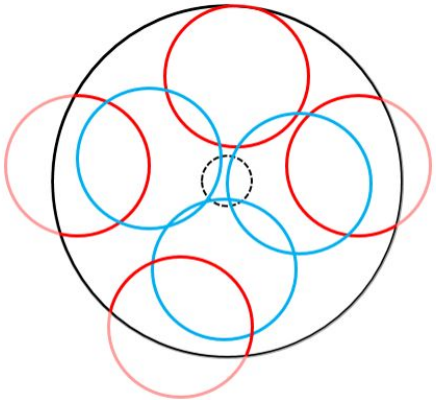

$B_3 >$

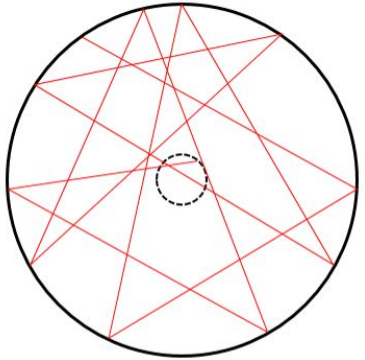

$B = 0$

$$1/\sqrt{|Q\,B|} \ll R \leqslant 1/\omega.$$

c=1

Causality mandates boundary to maintain
Tangential velocity < Speed of light
Bulk physics unaffected by boundary for
Strong enough magnetic fields
As magnetic length, l_B << system size

Boundary conditions make finite-size effects important only when $l_{\rm system} \lesssim l_B$ which corresponds to a very narrow sliver ($0 < eB \lesssim 0.0064$ GeV^2 for $l_B \sim l_{\rm system} = 12.5$ GeV^{-1} or 2.5 fm) in the phase space that we will investigate. Also, these distortions occur due to the so-called edge states and become essentially irrelevant in the deep interior, i.e., $r \ll R$, of the system where only the bulk states dominate. Depicted above, schematically

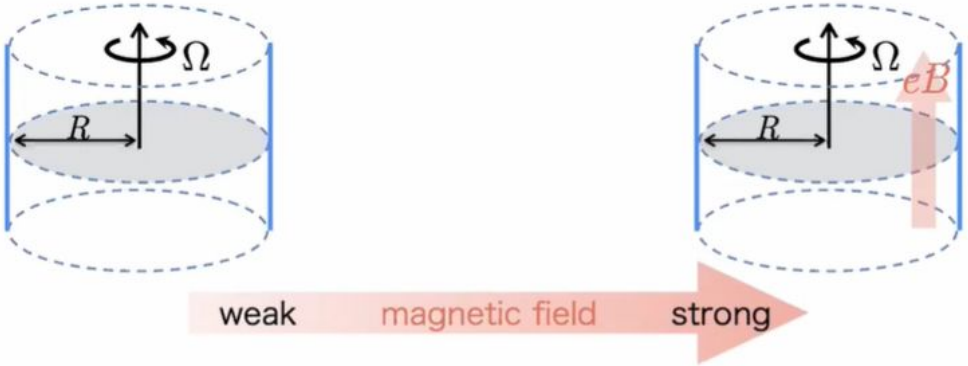

Kazuya Mameda, Rotational effect versus finite-size effect
Chen et al., Phys. Rev. D 93 (10) (2016) 104052

Momentum Discretization

Bosons in a well

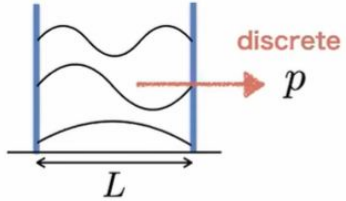

Dirichlet type

$$\sin(px)|_{x=L} = 0$$

$$\rightarrow \quad p = \frac{n\pi}{L} \geq \frac{\pi}{L}$$

IR gapped mode

Fermions in a cylinder

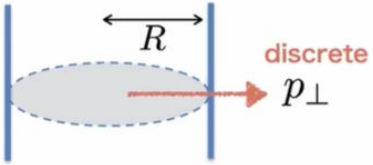

NO incoming current

$$\hat{e}_r \bar{\psi} \gamma^r \psi \Big|_{r=R} = 0$$

$$\rightarrow \quad p_\perp \mp \frac{\xi_{l,k}}{R} \geq \frac{\xi_{l,1}}{R}$$

IR gapped mode

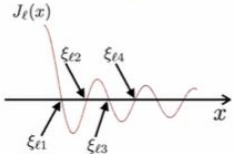

$\xi_{l,k}$: the kth root of $J_l(x)$

Results: parameter values chosen as should be *relevant for typical heavy-ion collisions*

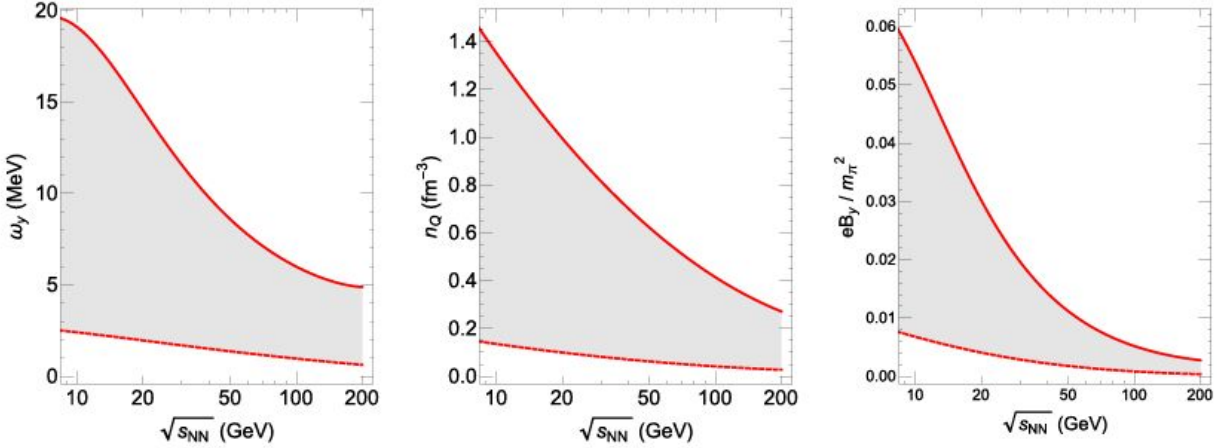

Figure 2. The vorticity ω_y (left, in unit of MeV corresponding to 1.5×10^{19} sec^{-1}), charge density n_Q (middle, in unit of $\mathrm{fm}^{-3} = 10^{45}$ m^{-3}) and magnetic field $e\overline{B}$ (right, in unit of m_π^2 corresponding to 3.3×10^{14} Tesla) as functions of collisional beam energy $\sqrt{s_{NN}}$ (in unit of GeV $= 10^9$ eV), with solid/dashed curves in each panel representing an upper/lower estimates and with the shaded band between them giving an idea of the expected range **Guo et al., 2020**

key result that connects the magnetic field with the vorticity:

$$e\overline{B} = \frac{e^2}{4\pi} n(\pi R_0^2)\overline{\omega} = \frac{e^2}{4\pi} nA\overline{\omega}$$

n: charge density, A: transverse area

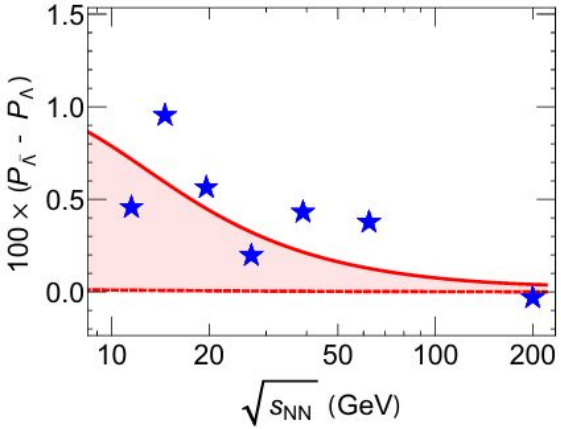

Figure 3. The induced polarization difference between hyperons and anti-hyperons, $\Delta P = P_{\bar{\Lambda}} - P_\Lambda$ as a function of collisional beam energy $\sqrt{s_{NN}}$ (in unit of GeV $= 10^9$ eV), in comparison with STAR data[47]. The solid/dashed curves are obtained from the upper/lower estimates for $e\overline{B}$ (see solid/dashed curves respectively in Fig. 2 right panel).

Momentum Discretization

Bosons in a well

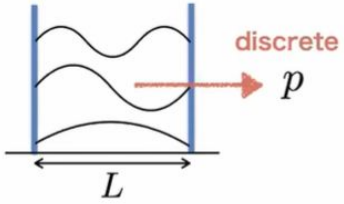

Dirichlet type

$$\sin(px)|_{x=L} = 0$$

$$\longrightarrow \quad p = \frac{n\pi}{L} \geq \frac{\pi}{L}$$

IR gapped mode

Fermions in a cylinder

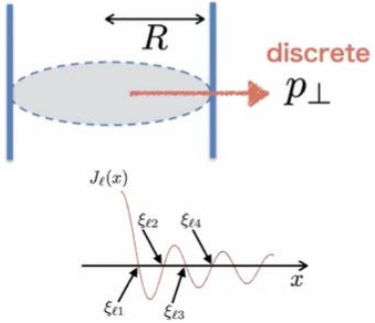

NO incoming current

$$\hat{e}_r \bar{\psi} \gamma^r \psi \Big|_{r=R} = 0$$

$$\longrightarrow \quad p_\perp \mp \frac{\xi_{l,k}}{R} \geq \frac{\xi_{l,1}}{R}$$

IR gapped mode

$\xi_{l,k}$: the kth root of $J_l(x)$

Kazuya Mameda, Rotational effect versus finite-size effect
Chen et al., Phys. Rev. D 93 (10) (2016) 104052
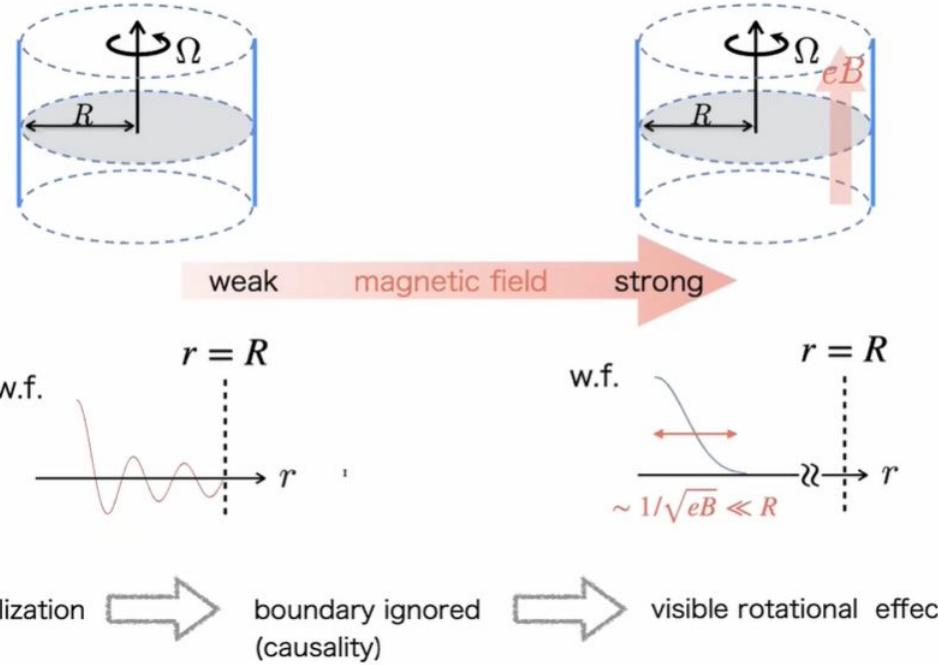
Gapped to Gapless